

**Using a High-Resolution Bog Sediment Core at Tamarack Pond,
NY to Constrain an Extraterrestrial Impact in the Hudson
Region ~2300 yr. B.P.**

Ronnie Phillips, Lamont Doherty Earth Observatory of Columbia University, Palisades, NY 10964

Project Advisors: Dallas H. Abbott, Kim Kastens, Terry Plank

Lamont Doherty Earth Observatory of Columbia University, Palisades, NY 10964

ABSTRACT

We examined a bog sediment core from Tamarack Pond, NY for evidence of impact ejecta around a previously constrained age horizon of 2300 yr. B.P. This horizon approximately coincides with a tsunami event recorded in sediment cores from Long Island and in the Hudson River, which some hypothesize was triggered by a hypervelocity bolide impact on the eastern North American continental Margin. We attempted to determine whether a connection existed between the cores at Tamarack Pond and the characteristics of a potential candidate for an impact site in Carteret Canyon offshore New Jersey. We detected shocked minerals—including quartz—in the Tamarack Pond core as well as several spherules with great disparity in size, texture and color. We considered the layer containing these grains to be the ejecta layer; however a thickness of 6 cm was several orders of magnitude greater than the ejecta layer thickness predicted by a computational model, using Carteret Canyon as the impact site. The reasoning for this discrepancy may be related to bioturbation or the model's failure to accurately represent processes that affect the distribution of distal ejecta.

TABLE OF CONTENTS

ABSTRACT	2
INTRODUCTION	5
Study Site: Tamarack Pond, NY.....	6
Crater Candidate: Carteret Canyon.....	6
Hudson Impact-Triggered Tsunami Event.....	7
Project Goals.....	7
BACKGROUND	8
Impacts and Shock Metamorphic Effects.....	8
Other Ejecta Types.....	10
METHODS	11
Sampling Scheme and Analysis.....	11
Computer Models.....	12
OBSERVATION AND DISCUSSION	13
Shocked Minerals.....	13
Alumino-oxide Minerals.....	15
Spherules.....	16
Other Minerals and Glasses.....	16
Radiocarbon Dating Results.....	17
Predicted and Observed Ejecta Layer Thickness.....	18
Bioturbation.....	20
CONCLUSION	21
Further Work.....	22
REFERENCES	24

LIST OF FIGURES.....	28
FIGURES.....	30
LIST OF TABLES.....	49
TABLES.....	50
APPENDIX I: Grain SEM Analysis Log.....	55
APPENDIX II: Additional Shocked Minerals.....	60
APPENDIX III: Additional Spherules.....	63

Introduction

Although the celestial dance of interplanetary bodies has captured the imagination of humanity for millennia, rigorous studies of the Earth's interaction with extraterrestrial objects such as asteroids and comets did not begin until a little more than a century ago when the Barringer crater in Arizona was first recognized and documented as a terrestrial impact site. Since then, geoscientists have built up an arsenal of diagnostic tools for identifying the occurrence of impact events in the stratigraphic record.

Extraterrestrial impacts impose both macroscopic and microscopic changes in target rocks. As the impactor transfers its kinetic energy into the host rock at contact, intense pressures and temperatures are generated in the subsequent shock wave that forms. These peak pressures and post shock temperatures can range from ~2 GPa near the crater rim to >100 GPa near the impact point and 500° to 3000°C in the surrounding rock to as high as 10,000°C near the impact point, respectively (Table 1), far outside the range of values produced in normal equilibrium metamorphic processes (typically <1-3 GPa and <1000°C; e.g., French, 1998). The exact shock wave pressure and post shock temperatures depend on the density of target rock, the latter being significantly higher in more porous rocks (e.g., Stoffer, 1984). This is because part of the shock wave's energy during impact is absorbed by compressing the pore space in the target rock, leading to a higher postshock temperature and a lower peak pressure required to induce melting.

Extraterrestrial impacts have played a prominent role in the geological and biological history of the planet, and yet the study of them has been heavily biased. Of the 170 or so impact structures on Earth known to geoscientists (Impact Database), less than 20% are now submarine (Gersonde et al., 2002), both because of the bias toward detection of terrestrial impact sites and because time and tectonic processes like subduction tend to erase older structures. Thus, an impact-triggered tsunami event recorded in the Hudson region with an associated submarine crater becomes an important contribution to the present record of oceanic impacts.

Study Site: Tamarack Pond, NY

Originally a bog, Tamarack Pond (Figure 1) was artificially converted from a bog to its present form within the last century. It is located near Cornwall, NY within the Black Rock Forest region of the Hudson Highlands (Figure 2). The relatively high sedimentation rate (roughly 1 mm/year; Gerard-Little et al., 2008) of the bog makes the setting ideal for studies where age constraint is important, though the effects of bioturbation must be considered. Tamarack Pond has been the site of a previous study that aimed to determine whether high resolution cores could be used as impact indicators by looking for discrete ejecta layers within a sediment core from the site (Gerrard-Little et al., 2008). Gerrard-Little et al. found quartz with large Fe-Ni-Cr splashes across its surface and possible planar deformation features at a core depth of 495-497 cm (Gerard-Little, 2008; Abbott et al., in press), the former feature associated with the Ries impact crater in Germany on the same scale (El Goresy and Chao, 1976), and the latter a common indicator of impacts (French, 1998). However, further work is needed to confirm that the quartz is indeed shocked, including examination of the orientation of the PDFS in reference to the crystallographic axes. Shallower depths (~492 cm and ~482 cm) have yielded basaltic glass and ilmenite with lead splash and carbon glass potentially containing impact diamonds, respectively (Abbott et al., in press). Radiocarbon dating of organic material from the 495-497 cm depth interval constrained its date of origin to approximately 311 +/- 100 BCE (Gerard-Little et al., 2008).

Crater Candidate: Carteret Canyon

A prospective location for an impact crater in Carteret Canyon on the eastern North American continental shelf about 310 km southeast of Tamarack Pond (Figure 2; Figure 3) was identified (Dallas Abbott, personal communication) by an unusually circular headwall upslope from a depression with exposed Middle Eocene deposits, until present speculated to be a plunge pool (Farre, 1985). The depression is at a depth of 1800 meters below sea level with a maximum depth of about 100 meters (Figure 4a) and measures roughly 860 meters in diameter (Figure 4b)(Farre, 1985). The lithologic

description of Middle Eocene deposits from the DSDP612 core drilled 6.6 km away from the depression calls the exposed unit carbonate-rich biosiliceous ooze and chalk (DSDP database from Farre, 1985), while that of the DSDP 108 core describes Middle Eocene deposits siliceous and calcareous limestone (Hollister et al., 1972 from Farre, 1985).

Hudson Impact-Triggered Tsunami Event

Goodbred and colleagues (2006) identified an occurrence of fining-upward sand and gravel deposits in a lagoon within Long Island's Great South Bay (Figure 2). Radiocarbon dating showed that the sand and gravel had been deposited contemporaneously with reworked shell beds and erosional surfaces in the area and gave the depositional event an age of 2300 yr. B.P. Because they were observed to occur over hundreds of meters laterally and only 1-2 meters vertically, the deposits are associated with a sudden, high-energy event consistent with a tsunami (Goodbred et al., 2006).

Further work on the layer came from samples taken from sediment cores at the bottom of the Hudson River near Piermont, NY (Cagen et al., 2008)(Figure 2). Cagen and colleagues identified carbon and aluminosilicate spherules, shocked illmenite and olivine, aluminosilicate glasses and nanodiamonds—specifically, lonsdaleite—within the layer.

Other high-energy events that might have produced such a deposit such as a turbidity flow or large storm seem unlikely, given the roughly 75 km distance between Great South Bay, NY and Piermont, NY and the presence of impact-produced spherules and shocked minerals within the deposits.

The rapid and widespread deposition of these layers, combined with the presence of impact spherules and shocked minerals, suggests that perhaps the tsunami was generated by an extraterrestrial impact. Discovery of any material from this Hudson impact event (so named because the first impact-associated material was found in the Piermont core on the Hudson River) in the Tamarack Pond core would further support this hypothesis.

Project Goals

The aim of this project was to first show demonstrable evidence of impact ejecta within the core from Tamarack Pond and if possible a correlation to the ejecta-rich tsunami layers in cores from the Hudson region and near the crater candidate by either composition or age. Determination of the ejecta layer's thickness in Tamarack Pond and consideration of any dateable organic material would offer a further constraint of the age of the impact. Analysis of ejecta will contribute to the accumulating catalog of Holocene impact events and further study of how the Earth interacts with extraterrestrial objects.

Background

Impacts and Shock Metamorphic Effects

Impact scientists have identified a variety of shock metamorphic effects on both the microscopic and macroscopic scale, though for the purposes of this study, we have focused primarily on microscopic features. These include planar deformational features (PDFs) on mineral surfaces, Brazil twinning, kink-banding, the presence of diaplectic glasses (e.g., Figure 5) or high –pressure polymorphs; each corresponds to an approximate shock pressure and postshock temperature (Table 2; French, 1998 from Stöffler, 1984). Also indicative of impact events is the presence of impact spherules or tektites (French, 1998)(e.g., Figure 6).

Shock metamorphism was first observed in quartz grains from the Clearwater Lake impact site in Quebec (McIntyre, 1968), and since then, shocked quartz has come to represent within the scientific community the unequivocal indicator of an impact event. Conveniently, quartz is often a constituent of most terrestrial crustal rocks and is very resistant to weathering, making it a valuable impact indicator for a variety of target substrates and ages. The relatively high strain rates, peak shock pressures, and postshock temperatures—compared to normal geologic metamorphic processes (Table 2)—actually deform the structure of the mineral's crystal lattice along individual planes and present as multiple sets of closed, narrow (<2-3 μm), closely spaced (2-10 μm) parallel features known as PDFs (Goltrant et al.,

1991; French, 1998)(Figure 7a). As many as eight intersecting sets have been recognized optically in shocked quartz samples (Mark Anders, personal communication). Though PDFs can also form due to tectonics, these tend to form curved rather than straight lines, indicating a more gradual process (Figure 7b). PDFs are a common way of identifying shocked silicate minerals, as they are more widely distributed than the high pressure polymorphs of quartz—another impact indicator that is especially persuasive when occurring with diamond or with silica glass and quartz—and are simpler to recognize (French, 1998). PDFs have been observed in other minerals besides quartz and feldspar, including pyroxene, amphiboles, garnet, and zircon (Stöffler, 1972), but as these minerals are not as prevalent in crustal rocks, little is known about their formation and crystallographic orientations.

The conventional method for confirming shocked minerals requires that prospective grains be made into thin section slides for electron backscatter diffraction (EBSD) analysis. While the presence of PDFs is a compelling factor in identifying shocked grains, EBSD imaging allows for analysis of the orientation of the grain's crystallographic axes. Because PDFs tend to form along specific planes in the quartz crystal lattice (French, 1998), the pole normal to the impact-generated PDFs makes specific angles to the quartz grain's c-axis (Table 3). PDFs tend to form at pressures between about 8 and 25 GPa (French, 1998) and these angles can be used to further constrain the peak shock pressure of the shockwave that traveled through the mineral (Stöffler and Langenhorst, 1994).

The macroscopic scale effects of an impact, such as shatter cones, distinctively curved and striated fractures that resemble cones that are produced by the relatively lowest pressures of the impact. They can form in all target rock types and are usually found in below the crater floor or in the central uplifts of complex craters. Their formation is not entirely understood, nor is the reason why they are well-formed at some impact sites and not at others. Though scientists have more extensively studied the shatter cones that occur in terrestrial craters, they can occur in submarine craters (Suuroja et al., 2000). Shatter cone size ranges from hand specimen to outcrop. So far no bathymetric studies in

or around Carteret Canyon have indicated or even been designed to search for evidence of shatter cones.

Other Ejecta Types

Impact spherules are glassy objects produced when the target rock, melted by the high postshock temperatures produced by the peak pressures of the impact shockwave, is ejected at high velocity from the terrestrial crater, cooling rapidly during transport (Glass, 1998) (Figure 6), though the timing of their formation in the impact process is not well understood. One possible mechanism is that spherules form during ejection of superheated, highly shocked melt during the initial contact between the impactor and the target rock; another suggests that distribution of shock-melted material occurs during the expansion of the vapor plume after this initial contact (French, 1998). There are some related objects, such as tektites, glassy impact melt of target rock composition with distinctive spheroid, dumbbell, or teardrop morphology and a similarly mystifying formation origin. Spherules often contain geochemical signatures which allow their source crater to be located (French, 1998; Jones-Zimmerlin et al., 2006), and can be radioactively dated to establish the age of the event (French, 1998; Hawkins, 1964). These glass melts are associated with distal ejecta deposits which may be distributed several crater radii (generally >5 radii) away from the impact site (Glass, 1998; French, 1998). A somewhat problematic feature of microspherules is that they have many sources: terrestrial (biogenic, diagenic, industrial, volcanic) and extraterrestrial (interstellar and interplanetary dust, meteoritic airbursts) and cosmic impact melt (Raukas, 2000).

Diaplectic glass forms when the passing shockwave converts the entire crystal to an amorphous glassy phase (Figure 5). This occurs at higher shock pressures (35-45 GPa) than those that produce PDFs (Table 2), although they still preserve the original crystal textures and mineral fabric (French, 1998). More common examples of diaplectic glasses are plagioclase feldspar glass, known as maskelynite, and quartz glass.

Shocked minerals, impact spherules or tektites, diaplectic glasses, and grains with metallic splash occurring in an above average concentration are all considered to be deposited as part of bulk impact ejecta material (Montanari and Koeberl, 2000).

Methods

Sampling Scheme and Analysis

The C-14 dates already attained on plant macrofossils at the 495-497 cm depth interval of Tamarack Pond (Gerrard-Little, 2008) enabled us to develop a sampling scheme focused on layers immediately above and below the age horizon of the proposed impact event. One two-centimeter (8 cc) sample was extracted from each depth interval between 482 cm and 498 cm of the Tamarack Pond core, comprising 9 two-centimeter samples. Later we took five additional samples from the Tamarack Pond core, at the 480-482 cm, 492-494 cm, 494-496 cm, 498-500 cm, 500-502 cm depth intervals. Each sample was weighed on a Mettler Toledo balance and then wet-sieved through brass sieves of sizes 150 μm , 63 μm , and 38 μm before being allowed to air-dry. Due to time constraints, the later five samples were oven-dried at 60°C. Sieves were then unloaded with a special brush to prevent contamination from other samples, again weighed, and stored in labeled vials for future examination. Any dateable organic material was removed before sieving and sent out to the Lawrence Livermore National Laboratory's Center for Accelerator Mass Spectrometry for AMS C-14 dating.

Each sample was analyzed under a Leica optical microscope for the purpose of characterizing the appearance of inorganic, lithic grains with the aim of optically determining whether features that might indicate shock metamorphism were present. In addition to blind observation in which we intentionally concealed the depth interval that we were observing, the initial strategy was to look for lithic grains with a milky appearance, which we hypothesized might indicate altered internal crystal structure caused by multiple sets of shock lamellae. To test this hypothesis, a representative group of clear, translucent, and milky grains from each depth interval were placed on SEM mounts for analysis.

Other features indicative of impact include metallic splash or inclusions and the presence of diaplectic glass; prospective glasses, which exhibited concoidal fracture and not thought to be quartz, were also placed on mounts. Prospective spherules were also placed on mounts for SEM analysis.

Each mount was analyzed with a scanning electron microscope (SEM) equipped with energy-dispersive X-ray spectroscopy microanalysis (EDAX) for compositional analysis of mineral grains as well as electron back scatter diffraction and secondary electron settings for imaging. The composition and any features such as shock lamellae (Figure 7a), quench textures (Figure 8), or unusual cleavages that might indicate shock metamorphism were recorded and imaged. Images were taken in the most appropriate mixture of low-energy secondary electron (which shows structural differences, where steeper surfaces are brighter than flat surfaces) and high-energy backscatter electron (which shows compositional differences, where heavier elements appear brighter than light elements) modes to highlight specific features.

All lithic grains from each depth interval were placed on double-sided tape and mounted on petrographic slides to be made into thin section slides. Spherules were not included as they are too delicate to withstand the grinding process of slide-making. The thin sections were then examined with a Leica DMLP DFC420-equipped petrographic microscope and then subsequently polished and analyzed with an SEM in EBSD mode.

Computer Models

Several computational models exist to predict the distribution of ejecta from an impact event (e.g., Collins et al., 2005; O'Keefe and Ahrens, 1985; Artimieva and Morgan, 2009). That of Collins and Melosh (2005) allows the user to input data on a particular impactor, such as its speed, density, diameter, as well as the target substrate and impact angle. The model then provides such information as the dimensions of the impact crater as well as the thickness of the ejecta layer at a given distance. It is in this manner that the model is applicable to this project: given the known diameter and depth of

the crater candidate in Carteret Canyon, one can determine the expected thickness of the ejecta layer at Tamarack Pond for different kinds of impactors. However, the models' ability to accurately calculate the distribution of distal ejecta is not always guaranteed, as shall be discussed below.

Observations and Discussion

Shocked Minerals

Several shocked mineral candidates were identified through SEM analysis (Table 4). Though the bulk compositions of these minerals ranged from SiO₂ to alumino-oxide, the diameters of those grains that were measured were clustered around 60-70 μm, straddling the >38μm and >63μm sieve size fractions.

Prospective shocked quartz grains were identified on the basis of straight, parallel PDFs in at least one direction. Five such grains were detected through SEM analysis and subsequently sent out to be made into thin section along with the remaining lithic grains from their depth interval. Some, such as grain 251-25, were also accompanied by prospective "passenger" spherules (Figure 9a). The confidence in whether the characteristics of a grain are actually evidence of shock differs for each grain. For example, grain 257-20 provides compelling evidence of shock features: it has at least two and possibly more than three directions of intersecting PDFs, which are straight despite being on a curved surface, and fit the physical characteristics of shock-induced PDF formation (Figure 9b). In contrast, a less compelling example can be found in grain 257-24, which has sub-parallel and curved PDFs, possibly due to surface morphology (Figure 9c). A tectonic mechanism could also be responsible, although the spacing of the PDFs is still consistent with shock-generated PDFs.

PDFs sometimes create triangular features on the cross-section of the crystal (Figure 10a); these can indicate the presence of more PDF directions where only one might ordinarily be visible on a particular crystal face (Dallas Abbott, personal communication). These triangular structures were noted on a potassium feldspar mineral grain (257-32), and provided the basis for supposing the grain had

multiple directions of PDFs (Figure 10a). Another K-spar grain (253-27)(Figure 10b) had no obvious cleavage planes, which normally appear as small, shelf-like features (Figure 10c). This is unusual for feldspar, which suggested some kind of diagenesis. SEM analyses of the clear, white, and milky “representative” grains from each depth interval revealed no clear and simple pattern to optically selecting shocked minerals from samples based on these characteristics alone.

All grains potentially called shocked quartz came from the three depth intervals 492-494 cm, 494-496 cm, and 496-498 cm, while no other shocked quartz candidates were identified outside of these depth intervals. This 6 cm layer is what we are inferring to be the ejecta layer (Figure 11).

All prospective shocked grains were removed from the mounts after SEM analysis and sent out along with all of the remaining lithic grains from the samples to be made into thin section slides for EBSD. Only about 50% of the grains sent out to be made into thin section actually appeared on the slides, and there was no way of knowing which grains were from previous SEM studies, if any. No grains from the 492-494 cm, 494-496 cm, or 496-498 cm depth intervals appeared to exhibit shock characteristics either optically (Mark Anders, personal communication) or through SEM analysis. Given an already limited sample size of about 40 or so grains per size fraction per depth interval and that even in large impacts like the K-T Chicxulub event in some distal sites less than 5% of the estimated quartz grains were actually found to be shocked (Morgan et al., 2006), the likelihood of finding shocked quartz grains in a sample already reduced by 50% is very low. However, although it is the conventional method to confirm that minerals have been shocked through EBSD analysis of the minerals in thin section, some studies have been conducted optically or by SEM analysis (e.g., Bohor, 1990; Morgan et al., 2006).

The exposed substrate within the circular depression in Carteret Canyon contains siliceous limestone and chalks, so the presence of shocked quartz, derived from silicate-bearing target rocks, would not be unexpected. The size of shocked quartz grains decrease with distance from the impact site (Morgan et al., 2006) as does the mean size of bulk ejecta (French, 1998). That is, smaller grains are

transported further. The average size of a prospective shock quartz grain from Tamarack Pond is about 65 μm , while that of candidate shocked quartz grains recovered from core ATII-124-11 near Carteret Canyon are greater than 150 μm (Dallas Abbott, personal communication). No shocked quartz grains have been yet found in any of the Hudson cores (Cagen, 2008; Abbott, in press). The next step will be to examine cores from the other side of Carteret Canyon from Tamarack Pond to see if the average size of shocked quartz grains increases outward from the crater candidate.

We also hypothesized that an impact event might produce a large influx of lithic grains into Tamarack Pond, and that we might be able to detect the presence and thickness of the ejecta layer based solely on the abundance of lithic grains. However, this was found not to be the case, as there appeared to be no correlation between grain abundance and depth (Figure 12).

Alumino-oxide Minerals

Two other alumino-oxide minerals were recovered with shock characteristics but uncertain composition (251-24; 257-28). 251-24 features at least two directions of PDFs with a spacing of 9 nm (Figure 13a); 257-28 had at least two directions of PDFs with 2 μm spacing (Figure 13b). These minerals were also sampled from the 492-494 cm, 494-496 cm, and 496-498 cm depth intervals. Other unshocked alumino-oxide minerals were analyzed, each with varying compositions of carbon, aluminum, and oxygen (Table 5). We hypothesized that comparing the chemical composition between the aluminosilicate grains from the Hudson cores and the alumino-oxide grains from Tamarack Pond might indicate something about the relationship between those locations. That is, if there were some kind of continuum in the composition of shocked aluminum-oxide-silicate grains that varied with distance from the source of the impact (in this case, Carteret Canyon), that might be evident in the comparison of grain composition between the Hudson and Tamarack Pond cores. However, in examining the composition of the alumino-oxide grains in the Tamarack Pond core alone, there appeared to be no correlation between composition and depth, based on the atomic weight ratios in each grain (Table 5).

Perhaps the composition within these alumino-oxide minerals in Tamarack Pond is too variable to isolate any kind of chemical trend, or there may be no correlation.

Spherules

Twelve carbon-rich spherules were found throughout the Tamarack Pond samples. Half of these spherules had a diameter between 35 and 40 μm (Table 4), but surface texture varied between smooth (Figure 14a) and pitted (Figure 14b). Other than an impact origin, carbon spherules can also be formed in forest fires or due to pollution. Given the timing of this proposed event, the production of carbon spherules via pollution seems unlikely. However, given the regularity of forest fires in the Black Rock Forest region, this mechanism for production of carbon spherules cannot be ruled out. The disparity in texture, color, and size, as well as the pervasiveness of the spherules throughout the sample depths, including the layer postulated to be the ejecta layer (Figure 11), might indicate that more than one mechanism is responsible for the presence of the carbon spherules in Tamarack Pond. At present, not enough is understood about carbon spherule formation to decouple these mechanisms.

Other Minerals and Glasses

Glasses can be identified optically in thin section with a petrographic microscope, as they appear black in cross-polarized, transmitted light. We detected no promising glass particles in the thin section slides.

Grains rich in chromite were included in the table for the purpose of categorizing the nonbiogenic grains that were analyzed, but at present a source for the chromite is unknown. It could possibly be part of the original impactor, given that a higher proportion of the impactor would be deposited as distal ejecta (French, 1998). This means that a greater fraction of distal ejecta would be composed of bits from the impactor itself, compared to proximal ejecta. Chromite is also produced because cosmic objects can form the chromite spinel end member during atmospheric entry while terrestrial crustal material tends to be Cr-depleted (Robin et al., 1991). Because the chromite-rich grains

occur in the 488-490 cm and 494-496 cm depth intervals, the shallower not being part of the inferred ejecta layer, we interpret them as having been locally derived from the Precambrian metamorphic and igneous crystalline basement rock (Figure 11). Chromite-rich grains have not been found in any of the Hudson cores from the tsunami layer (Dallas Abbott, personal communication), further supporting the hypothesis that the chromite is from a local source.

A CaCO₃ foram found in the Tamarack Pond sample (Figure 15a; Figure 15b) is from the 492-494 cm depth interval, also containing prospective shocked minerals, has been identified as of the *Ammonia* genus, an inner neritic benthic foram usually found in brackish water (Stever Pekar, personal communication). Foraminiferal assemblage studies of the Hudson Estuary show no foraminifera species inhabiting the river at the sample station nearest to Tamarack Pond (West Point, see Figure 3) (Weiss et al., 1977). According to the Weiss (1977) study, *Ammonia* foraminifera prefer the more brackish water of the Hudson Estuary between the river near upper Manhattan and Piermont, NY. It is possible that the foram found in the Tamarack Pond sample is contamination from Piermont samples or that it was dropped by, say, a bird; with only one foram found it is hard to make the case either way, since the author is not supposing the tsunami reached Tamarack Pond.

The first SEM analysis yielded anomalous patches of copper and zinc on many of the samples; these patches were later attributed to the brass sieves.

Radiocarbon Dating Results

Previous AMS Carbon-14 dating of organic material in Tamarack Pond at relevant depths consisted of two water lily seed fragments and two aquatic *brasinia* seeds from the 495-497 cm depth interval, identified by Dr. Dorothy Peteet (Gerrard-Little, 2008). These yielded central radiocarbon ages of 2305 ± 35 and 2340 ± 35 years and calibrated central dates of 311 BCE ± 100 years and 391 BCE ± 130 years. The present study recovered additional organic material from the 500-502 cm depth interval: one sedge family *Cladium mariscoides* seed and three *Brasenia schreberi* (also known as watershield) seeds

have been identified by Dr. Dorothy Peteet and radiocarbon dated (Table 6). These samples returned a central ^{14}C age of 2310 ± 35 years. The calibrated age of 2350 ± 15 years provides a lower stratigraphic constraint on the date of the impact event that these compelling shocked minerals seem to be suggesting, well within of the age of tsunami on the eastern margin.

Predicted and Observed Ejecta Layer Thickness

Based on the presence of shocked minerals identified by SEM analysis, the thickness of the ejecta layer in Tamarack Pond is suggested to be about 6 cm, between 492 cm and 498 cm (Figure 11). The contribution of the carbon spherules and chromite grains is complicated by the inherent uncertainty of carbon spherule formation and chromite origin (Figure 11).

For a typical comet, C-class (less dense) asteroid, S-class (denser) asteroid, and Fe-rich asteroid impact likely to produce the type of structure of the crater candidate in Carteret Canyon, Collins' computational model predicted almost no solid ejecta at the distance of Tamarack Pond, 310 kilometers (Figure 16). To obtain these calculations, we took the current dimensions and depth of the circular depression in Middle Carteret Canyon indicated by bathymetric data to be the dimensions of the final impact crater. Using the typical impact angle (45°) and impact speed (~ 50 km/s for comets and ~ 17 km/s for asteroids), we manipulated the size of each type of impactor until it produced a crater matching the dimensions of the depression in Middle Carteret Canyon (Table 7). Then we input different distances from the crater into the model and calculated how thick the ejecta layer would be at that distance and thus the radial extent of the ejecta layer. We found that an ejecta blanket of micron thickness terminates at 111.25 km, 83 km, 122 km, and 113 km for a comet, C-class, S-class, and Iron asteroid, respectively (Figure 16).

However, many models of ejecta distribution do not accurately predict the distribution of distal ejecta deposits (Artemieva and Morgan, 2009). This may be due to their well known lack of ability to represent vaporization geologic materials (Artemieva and Morgan, 2009), of which distal ejecta is mostly

comprised, or because they only consider ballistic transport mechanisms (Collins et al., 2005 from Ahrens and O'Keefe, 1978) when some scientists now think that a non-ballistic mechanism for particles such as shocked quartz better matches observational data of shocked quartz distribution in ejecta deposits (Artemieva and Morgan, 2009), or because they do not incorporate atmospheric turbulence or wind patterns (Collins, 2005), which would have a greater effect on smaller particles. Unlike the ballistic mechanism where transport is airborne and free from confining pressures, the non-ballistic mechanism transports particles via roll and glide motions in high confining pressures along the surface, and particles can move relative to one another during transport (Chao, 1976). For the Collins et al. (2005) model, the volume of melt ejecta deposited beyond the final crater rim is governed the volume of material within the transient crater subjected to a certain pressure, and ejecta distribution for smaller impacts ($E < 200$ Mt TNT) is dependent on the radius of the fireball (the expanding vapor plume) produced in the impact. Larger impacts produce fireballs with radii larger than the scale height of the atmosphere, so ejecta escape the dense part of the atmosphere and are able to travel further distances (Collins et al., 2005). Radial ejecta thickness for the Collins et al. (2005) model was based on semi-empirical data of lunar craters (McGetchin et al., 1973), which, given that the Moon is without an atmosphere, might not provide the best analogue for terrestrial impacts. The ejecta layer is thickest at the rim of the transient crater and decreases roughly as one over distance cubed (McGetchin et al., 1973; Collins et al., 2005)

To test how accurately the Collins (2005) predicts the thickness for an ejecta layer for which there are observational data, namely the Chicxulub impact, known parameters based on observed or empirical data, were input into the model and the predicted thickness of the ejecta layer was determined for a range of distances, proximal and distal, and then compared to the observed thicknesses at comparable distances (Figure 17). While the thickness of the Chicxulub ejecta layer is not constant with distance, there are a few well studied sites with relatively undisturbed layers, and the radial thickness for a given distance is generally within the same order of magnitude (Smit, 1999). For

each proximal (2500 km), intermediate (2500-4000 km), and distal (7000 km) location, the model predicted ejecta thicknesses within the range given by observational data. However, for the more distal, global location from Woodside Creek, New Zealand, where the observed thickness is a few mm thick (Smit, 1999), the model gives a thickness less than 1 mm. The model's range for an ejecta layer thicker than 1 mm extends to about 9500 m from the impact site (Figure 17).

This particular model appears to predict ejecta layer thicknesses fairly accurately until a certain point; the more distal layers are underestimated, perhaps implying that a more distal site like Tamarack Pond from an impact site at Carteret Canyon is also underestimated. The minimum thickness of the predicted ejecta layer in the Collins et al. 2005 model is at the micron level, so even an overestimate of one order of magnitude for Tamarack Pond—that is, predicting a layer of thickness in μm instead of a nonexistent layer—does not explain the 6 cm-thick layer observed in the Tamarack Pond core.

Using the Collins et al. 2005 model convention that the thickness of ejecta is related to the volume of target rock subjected to a given peak pressure value. We ran various types of impactors through the Collins et al. 2005 model to see how much melt volume was produced with a constant 6 cm-thick ejecta thickness at a distance of 310 km from the impact site, and found that less energetic impacts (i.e. denser impactors) produced less impact melt overall, but the same size crater and ejecta thickness as more energetic impacts (Table 8). For comparison the volume of the crater candidate is about 3 km^3 . The discrepancy between constant ejecta thickness but smaller melt volumes for less energetic impacts may be due to a greater transfer between impactor speed to kinetic energy in target rock at the surface, resulting in more ejecta from the surface, suggesting that ejecta thickness is also related to transient crater size (Figure 18).

Bioturbation

Perhaps there are other effects, such as bioturbation, which may have spread the layer out stratigraphically. Not much is known about bioturbation in this environment. Operating under the

assumptions that the ejecta layer was initially a discrete layer of lithic grains transported from the impact site and that none of the lithic grains from the inferred ejecta layer is local, we can approximate the original ejecta layer thickness by compressing all of the lithic grains from the inferred 6 cm-thick ejecta layer into a discrete layer and determining its thickness. We found that the minimum amount of lithic grains contained in the 6 cm by 2 cm by 2 cm rectangular prism that represents the samples we interpreted to be part of the ejecta layer, when spread out across the 4 cm² area, compress to a thickness of about one-quarter of a micron (Table 9). This may provide a new constraint for bioturbation in a bog environment, as it suggests that over the about 2300 years since this material was deposited here in an approximately discrete layer, the organisms in the bog actively spread it out over a vertical distance of about 6 cm.

Conclusion

A bog sediment core from Tamarack Pond, NY has recorded an impact event at about 2300 yr. B.P., evident in the presence of quartz and other mineral grains, detected through SEM analysis, that appear to have undergone shock metamorphism. Because they were not analyzed with EBSD in thin section, these quartz grains cannot be confirmed as shocked in the strict conventional sense of the scientific community; however, some studies have claimed to have detected shocked quartz optically and with the SEM. The timing of this impact event coincides with a tsunami event offshore New York which is believed to have been generated by an impact. At present no compositional connection has been established between the Tamarack Pond record and those recording the tsunami event in the Hudson, although the size profile of the shocked quartz grains in Tamarack Pond and near a crater candidate in Carteret Canyon suggest that the same impact at least in the direction of Carteret Canyon may be recorded in both locations. SEM analyses have prompted a suggested ejecta layer thickness of 6 cm at Tamarack Pond, which is several orders of magnitude thicker than predicted by Collins et al. 2005

computational model. This discrepancy may be due to the model's inability to accurately predict distal ejecta thicknesses or possibly bioturbation of an initially thinner ejecta layer.

Further Work

Having a more realistic idea of the sample size needed to detect shocked quartz grains and the average abundance of quartz grains per depth interval in the Tamarack Pond core, as well as an average size of shocked quartz grains, will allow future researchers to design a more favorable sampling scheme that considers the 50% grain turnaround of thin section slides. Still, given the significant effect of bioturbation on ejecta layer thickness, it may be more prudent to choose a high-resolution core that is free from this effect.

Etching quartz samples with HF acid has been shown to provide a less ambiguous distinction between PDFs formed by shock metamorphism and those resulting from normal tectonic metamorphism (Gratz, 1996). This will most likely be the next step with the limited quartz grain samples from Tamarack Pond.

Observational data of an ejecta layer thickness within a high-resolution core free from the effects of reworking or bioturbation may assist designers of computational models that predict ejecta distribution to better represent the impact processes taking place that produce distal ejecta, such as atmospheric or plume expansion dynamics. Additionally, the examination of high-resolution cores for smaller impact events may contribute to the understanding of impact rates and statistics of terrestrial impacts, a highly controversial concept (e.g., Asher et al., 1994; Asher et al., 2005; Melosh, 2007).

The 2300 yr. B.P. impact event is associated with a global climatic cooling observed in tree-rings around the same period, 207 BCE (Baillie, 1999; Baillie, 2007). There are a few somewhat well known climatic downturns that also cannot be explained by volcanism, including 536 CE. Definitive evidence of an impact during this timeframe in addition to an impact as suggested by the unconfirmed shocked

minerals in Tamarack Pond may help researchers understand the after-effects an impact can have on the atmosphere.

Another compelling impact event that possibly occurred within error of that in the Hudson is indicated by a crater strewnfield in southeast Bavaria, Germany, near the town of Chiemgau. The timing of this event is constrained by cultural artifacts and glass melts and is thought to be as old as 200 BCE and no younger than the first millennium BCE (Masse, 2007; CIRT). Shocked quartz has been found near the largest crater in the strewnfield. Development of a method to correlate the composition of shocked quartz spatially may allow researchers to detect and decouple the evidence of multiple, geologically simultaneous impacts.

Certainly multiple, geologically simultaneous impacts within the Earth-Moon system have been witnessed during recorded history, as exemplified by the boulder-sized impacts on the Moon on June 22-26, 1975 or the memorable break-up and subsequent impact of Comet Shoemaker-Levy onto the surface of Jupiter. This event—and others observed and noted in historical records within the Holocene—have been suggested to be associated with periods in which the Earth travels through a *cosmic swarm*—a term describing two or more objects having fragmented from their parent comet (Clube and Napier, 1990). The Earth encounters about 19 faithfully returning meteor showers every year (Hawkins, 1964), most of which are named according to the constellation—usually within the zodiacal cloud—from which they appear to originate (Clube and Napier, 1990; Hawkins, 1964) and some of which are associated with known cometary orbits (Hawkins, 1964). The paths of these streams generally follow that of their original parent comet, and the age of the stream can be inferred by the tightness of the cluster of cometary fragments (Clube and Napier, 1990). Fresh influxes of comets may occur as the solar system passes through the galactic spiral arms (Bailey et al., 1989), but the origins of comets are still not very well understood.

Acknowledgements

The author would like to thank Dallas Abbott for her boundless energy in pursuing this project, and Kim Kastens and Terry Plank for asking the important questions and keeping her on track; Dee Breger, the scanning microscopy *maestra*; fellow EESJ student Diya Chacko for moral support; Steve Pekar, Dorothy Peteet, and Mark Anders for their illuminating consultations; CCNY for the use of their SEM; the National Science Foundation and the Earth and Environmental Sciences Journalism Department at Columbia University for funding; Spectrum Petrographics for the mineral grain thin sections; and Tom Guilderson for the AMS C-14 dating.

References

- Abbott, Dallas; personal communication to Ronnie Phillips
- Abbott, D.H., P. Gerard-Little, Sa. Costa, St. Costa, D. Breger, and S. Haslett, in press, Proceedings of Tunguska Conference, Summer 2008, *Exotic Grains in a Core from Cornwall, NY--Do They Have an Impact Source?*
- Anders, Mark; personal communication to Ronnie Phillips
- Artemieva, N. and Morgan, Joanna. (2009) Modeling the formation of the K-Pg boundary layer. *Icarus*, 201, 768—780.
- Asher, D.J., Clube, S.V.M., Napier, W.M. and Steel, D.I. (1994) Coherent Catastrophism. *Vistas in Astronomy*, 38, 1—27.
- Asher, D.J., Bailey, M., Emel'yanenko, V. and Napier, W. (2005) Earth in the cosmic shooting gallery. *Observatory*, 25, 319—322.
- Bailey, M.E., Clube, S.V.M. and Napier, W.M. *The Origin of Comets*. Oxford: Pergamon, 1989.
- Baillie, Mike. *Exodus to Arthur: Catastrophic Encounters with Comets*. London: Biddles Ltd., 1999.
- Baillie, M.G.L. "Tree-Rings Indicate Global Environmental Downturns that could have been Caused by Comet Debris." *Comet/Asteroid Impacts and Human Society: An Interdisciplinary Approach*. Ed. Bobrowsky and Hans Rickman. Springer, 2007. pp. 105—122.
- Bohor, B.F. (1990) Shocked-induced microdeformations in quartz and other mineralogical indications of an impact event at the Cretaceous-Tertiary boundary. *Tectonophysics*, 171, 359—372.
- Cagen, K. and D. Abbott. 2009. Evidence for a tsunami generated by an impact event in the New York metropolitan area approximately 2300 years ago. Section I: 23 pp. In S.H. Fernald, D. Yozzo and

- H. Andreyko (eds.), Final Reports of the Tibor T. Polgar Fellowship Program, 2008. Hudson River Foundation.
- Chao, E.C.T. (1976) "Mineral-Produced High-Pressure Striae and Clay Polish: Key Evidence for Nonballistic Transport of Ejecta from Ries Crater." *Science*, 194: 615-618.
- Chiemgau Impact Research Team (CIRT) is: Rudolf Beer, Gerhard Benske, Thomas Bliemetsrieder, Dr. Kord Ernstson, Till Ernstson, Josef Lex, Hans-Peter Matheisl, Werner Mayer, Ernst A. Neugebauer, Andreas Neumair, Barbara Rappenglück, Dr. Michael A. Rappenglück, Ralph Sporn; website: <http://www.chiemgau-impact.com/index.html>
- Clube, Victor, and Bill Napier. *The Cosmic Winter*. Cambridge: Basil Blackwell Ltd., 1990.
- Collins, G.S., Melosh, H.J., and Marcus, R.A. (2005) Earth Impact Effects Program: A Web-based computer program for calculating theregional environmental consequences of a meteoroid impact on Earth. *Meteoritics*, 40, 6, 817—840.
- DSDP Database
- El Goresy, A. and E.C.T. Chao (1976), Evidence of the impacting body of the Ries Crater—the discovery of Fe-Cr-Ni veinlets below the crater bottom, *Earth and Planetary Science Letters*, 31, 330-340.
- Farre, J.A. (1985) *The Importance of Mass Wasting Processes on the Continental Slope*, PhD thesis, Columbia University
- French, Bevan M. *Traces of Catastrophe*. Houston: Lunar and Planetary Institute, 1998.
- Gerard-Little, P. and D. Abbott. (2008) Establishing a dated stratigraphy for a core from Black Rock Forest, Hudson Highlands, New York: Possible applications of distal impact ejecta as geologically instantaneous markers, senior undergraduate thesis, Columbia University
- Gersonde, R., Deutsch, A., Ivanov, B.A., and F.T. Kyte (2002) Oceanic Impacts—a growing field of fundamental geoscience. *Deep-Sea Research II* 49:951-957.
- Glass, Billy P. "Cenozoic Microtektites and Clinopyroxene-Bearing Spherule Layers in Marine Sediments." *Proceedings of the 1998 Annual Meeting TECOS (Terrestrial and Cosmic Spherules)*. Ed. Detre, Csaba H. Budapest: Akademiai Kiado, 1998. pp. 57—71.
- Goltrant, O., Cordier P., and Doukhan J.-C. (1991) "Planar deformation features in shocked quartz: A transmission electron microscopy investigation." *Earth Planet. Sci. Lett.*, 106, 103—115.
- Goodbred, S., Krentz, S., and P. LoCicero (2006) Evidence for a newly discovered 2300-year-old tsunami deposit from Long Island, New York. *Eos Trans. AGU* 87(53), Fall Meet. Suppl., Abstract OS43C-0681.

- Gratz, A.J., Fidler, D.K. and Bohor, B.F. (1996) Distinguishing shocked from tectonically deformed quartz by the use of the SEM and chemical etching. *Earth and Planetary Science Letters*, 142, 513-521.
- Hawkins, Gerald S. *Meteors, Comets, and Meteorites*. McGraw-Hill, Inc., 1964.
- Hollister, C.D., Ewing, J.I., Habib, J., Hathaway, J.C., Lancelot, Y., Luterbacher, H., Paulus, F.J., Poag, C.W., Wilcon, J.A., and Worstell, P. (1972). "Site 107 Upper Continental Rise and Site 108 Continental Slope." in, Hollister, C.D., Ewing, J.I., et al., *Initial Reports of the Deep Sea Drilling Project*, 11, Washington D.C.: U.S. Government Printing Office, pp. 351—363.
- Impact Database website <http://www.unb.ca/passc/ImpactDatabase/index.html>.
- Jones-Zimmerlin, S., Simonson, B.M., Kreiss-Tomkins, D., Garson, D. (2006) "Using impact spherule layers to correlate sedimentary successions: a case study of the Neoproterozoic Jeerinah layer (Western Australia)." *South African Journal of Geology*, 109, 1-2, pp. 245-261.
- Masse, Bruce W. "The Archaeology and Anthropology of Quaternary Period Cosmic Impact." *Comet/Asteroid Impacts and Human Society: An Interdisciplinary Approach*. Ed. Bobrowsky and Hans Rickman. Springer, 2007. pp. 25—70.
- McGethcin, T.R., Settle, M. and Head, J.W. (1973) Radial thickness variation in impact crater ejecta: implications for lunar basin deposits. *Earth and Planetary Science Letters*, 20, 226—236.
- Melosh, H.J. "Physical Effects of Comet and Asteroid Impacts: Beyond the Crater Rim." *Comet/Asteroid Impacts and Human Society: An Interdisciplinary Approach*. Ed. Bobrowsky and Hans Rickman. Springer, 2007. pp. 211—224.
- McIntyre, D.B. "Impact metamorphism at Clearwater Lake, Quebec." *Shock Metamorphism of Natural Materials*. Eds. French, B.M. and N.M. Short. Baltimore, Mono Book Corp., 1968, pp. 363—366.
- Montanari, A., and C. Koeberl (2000), *Impact Stratigraphy: The Italian Record*, Springer, Berlin.
- Morgan, J., Lana, C., Kearsley, A., Coles, B., Belcher, C., Montanari, S., Diaz-Martinez, E., Barbosa, A., Neumann, V. (2006) Analyses of shocked quartz at the global K-P boundary indicate an origin from a single, high-angle, oblique impact at Chicxulub. *Earth and Planetary Science Letters*, 251, 264—279.
- O'Keefe, J.D. and Thomas J. Ahrens. (1985) Impact and explosion crater ejecta, fragment size, and velocity. *Icarus*, 62, 2, 228—238.
- Pekar, Steve; personal communication to Dallas Abbott
- Raukas, A. (2000) "Investigation of impact spherules—a new promising method for the correlation of Quaternary deposits." *Quaternary International* 68—71, 241—252.

Reimer PJ, MGL Baillie, E Bard, A Bayliss, JW Beck, C Bertrand, PG Blackwell, CE Buck, G Burr, KB Cutler, PE Damon, RL Edwards, RG Fairbanks, M Friedrich, TP Guilderson, KA Hughen, B Kromer, FG McCormac, S Manning, C Bronk Ramsey, RW Reimer, S Remmele, JR Southon, M Stuiver, S Talamo, FW Taylor, J van der Plicht, and CE Weyhenmeyer. 2004 *Radiocarbon* 46:1029-1058.

Robin, E., Bonté, Ph., Froget, L., Jéhanno, C. and Rocchia, R. (1991) Formation of spinels in cosmic objects during atmospheric entry: a clue to the Cretaceous—Tertiary boundary event. *Earth and Planetary Science Letter*, 108, 181—190.

Ryan, Bill; personal communication to Dallas Abbott

Smit, J. (1999) The global stratigraphy of the cretaceous—tertiary boundary impact ejecta. *Annu. Rev. Earth Planet. Sci.*, 27, 75—113.

Stöffler, D. (1972) “Deformation and transformation of rock-forming minerals by natural and experimental shock processes: I. Behavior of minerals under shock compression.” *Fortschr. Mineral.*, 51, 256—289.

Stöffler, D. (1984) “Glasses formed by hypervelocity impact. *J. Non-Crystall. Solids*, 67,465—502.

Stöffler, D. and Langenhorst, F. (1994) “Shock metamorphism of quartz in nature and experiment: I. Basic Observation and theory.” *Meteoritics*, 29, 155—181.

Suuroja, Kalle and Surroja, Sten. “Neugrund Structure—the newly discovered submarine Cambrian impact crater.” *Impacts and the Early Earth*. Berlin/Heidelberg, Springer, 2000, pp. 389-416.

Weiss, D., Geitzenauer, K., and Shaw, F.C. (1978) Foraminifera, Diatom and Bivalve Distribution in recent Sediments of the Hudson Estuary. *Estuarine and Coastal Marine Science*, 7, 393—400.

List of Figures

Figure 1: Tamarack Pond near Cornwall, NY. Coordinates of Tamarack Pond: 41° 23' 43.45" N, 74° 01' 29.54" W

Figure 2: Study area with pertinent sediment cores highlighted in yellow: Tamarack Pond, NY (41° 23' 43.45" N, 74° 01' 29.54" W); light green: Great South Bay, NY (40° 40' 57.31" N, 73° 09' 15.40" W); green: Piermont, NY (41° 02' 34.88" N, 73° 53' 23.02" W), and red: the depression in Middle Carteret Canyon (38° 47.2' N, 72° 43.5' W). Created with Google Earth.

Figure 3: Location of crater candidate in Carteret Canyon (labeled in blue) and surrounding cores: ATII-124-11 (38° 47.598' N, 72° 43.002' W) in green, DSDP108 (38° 48' 20" N, 72° 39' 10" W) in yellow, and DSDP612 (38° 49.5' N, 72° 46.75' W) and red. Original bathymetry map from Farre, 1985.

Figure 4a: Cross-section of depression in Carteret Canyon. From Farre, 1985.

Figure 4b: Geological interpretation sketch of entire Carteret Canyon. Note circular headwall and depression at the division between Upper and Middle Carteret Canyon. From Farre, 1985.

Figure 5: Diaplectic glass from Chicxulub impact structure. Courtesy Calvin J. Hamilton.

Figure 6: Tektites and impact spherules from the K/T boundary in Haiti.

Figure 7a: Optical, plane-polarized light image of fresh, impact-generated PDFs in quartz from an impact structure in Sierra Madera, Texas. From French, 1998.

Figure 7b: SEM micrograph of Arkansas novaculite with tectonic (Boehm) lamellae, HF etched for three min. The lamellae appear solid and curved under the optical microscope. The box on the left is enlarge 3 X to create the picture on the right. From Gratz et al., 1996

Figure 8: Close-up of quench texture from an aluminosilicate spherule found in the Hudson study. From Cagen et al., 2008.

Figure 9a.1: (Grain 251-25) Micrograph of prospective shocked quartz grain with aerodynamic ablation of PDFs, spherule with passenger spherule and an interference pattern of PDFs.

Figure 9a.2: Micrograph close-up of PDFs on Grain 251-25.

Figure 9a.3: EDAX analysis of grain 251-25.

Figure 9b.1: (Grain 257-20) Micrograph of prospective shocked quartz grain. Straight PDFs on a curved surface, possibly 3+ directions of intersecting PDFs.

Figure 9b.2: EDAX analysis of grain 257-20.

Figure 9c.1: (Grain 257-24) Micrograph of prospective shocked quartz grain with melted surface, sub-parallel curved sets of PDFs that might reflect changes in surface morphology, irregular spacing.

Figure 9c.2: EDAX analysis of grain 257-24.

Figure 10a: (Grain 257-32) Micrograph of prospective shocked K-spar grain with distinctive triangular morphology possibly indicating PDFs.

Figure 10b: EDAX analysis of grain 257-32.

Figure 10c: Scanning electron micrograph of typical cleavage planes on a K-spar grain. Note directions of shelf-like features indicated by white lines. EDAX analysis shows K-spar composition.

Figure 11: Graph of abundance of shocked minerals, spherules, and other compelling minerals vs. depth.

Figure 12: Graph of abundance of lithic grains versus depth.

Figure 13a.1: (Grain 251-24) Micrograph of prospective shocked grain of aluminum oxide composition and lamellae 9 nm apart, possibly shocked kaolinite or corundum.

Figure 13a.2: EDAX analysis of grain 251-24.

Figure 13b.1: (Grain 257-28) Micrograph of prospective shocked grain, possibly corundum in composition.

Figure 13b.2: EDAX analysis of grain 257-28.

Figure 14a: (Grain 257-10) Micrograph of spherule with smooth texture.

Figure 14b: (Grain 251-15) Micrograph of spherule with "pitted" texture.

Figure 15a: Micrograph of foraminifera, Genus: Ammonia.

Figure 15b: EDAX analysis of foram.

Figure 16: Average solid ejecta thickness vs. distance for a comet, C-class asteroid, S-class asteroid, and iron-rich asteroid. Distance is in Final Crater Radii (R_{fc})= approximately 430 meters. Tamarack Pond, at a 310 km distance, is more than 720 R_{fc} from the crater candidate.

Figure 17: Thickness of proximal (2500 km), intermediate (4000 km), distal (7000 km), and global (15,000 km) ejecta, as observed (Smit, 1999) and predicted by computational model (Collins et al., 2005).

Figure 18: Locations of shock-metamorphosed materials in the transient crater. From French, 1998.

Figures



Figure 1



Figure 2

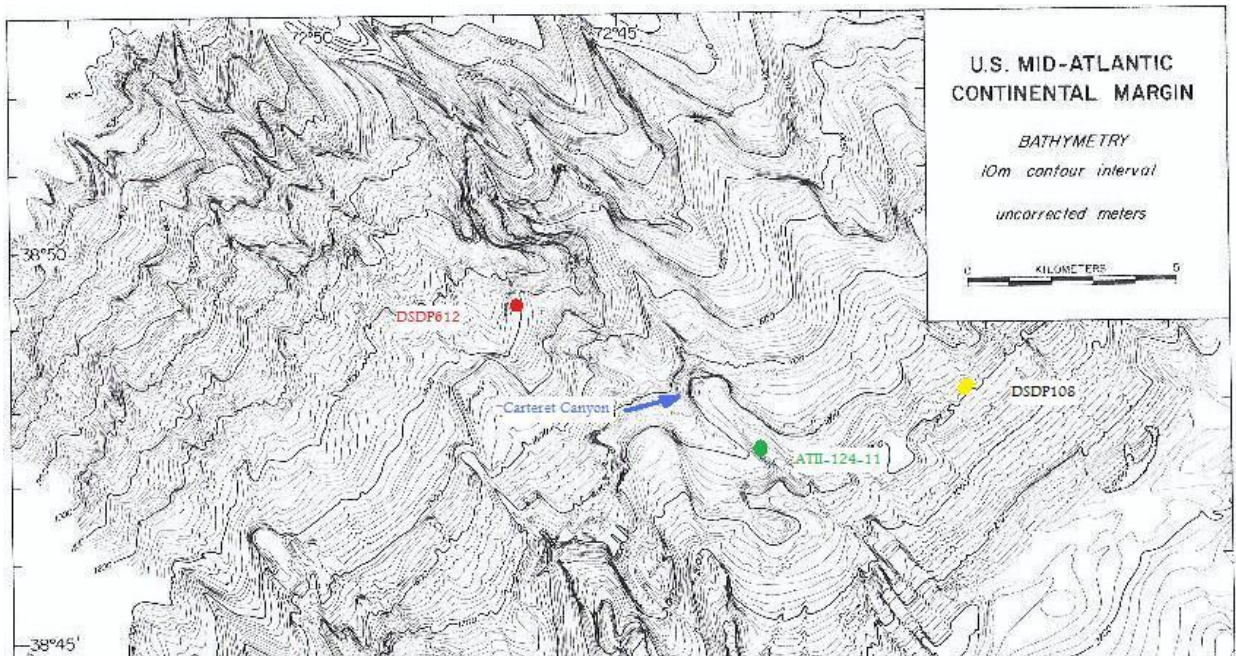


Figure 3

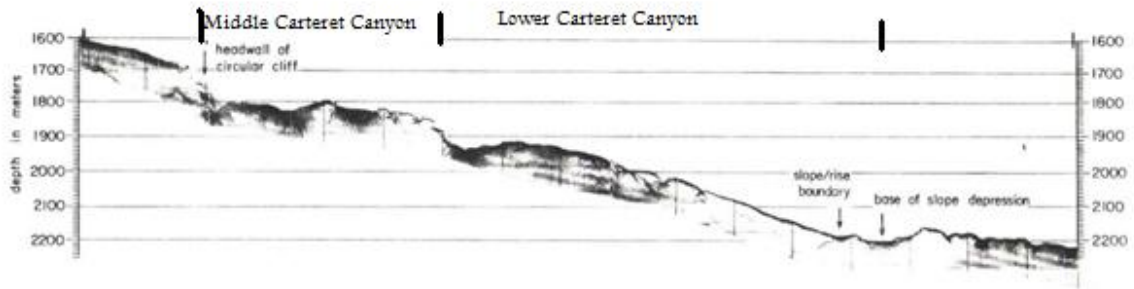


Figure 4a

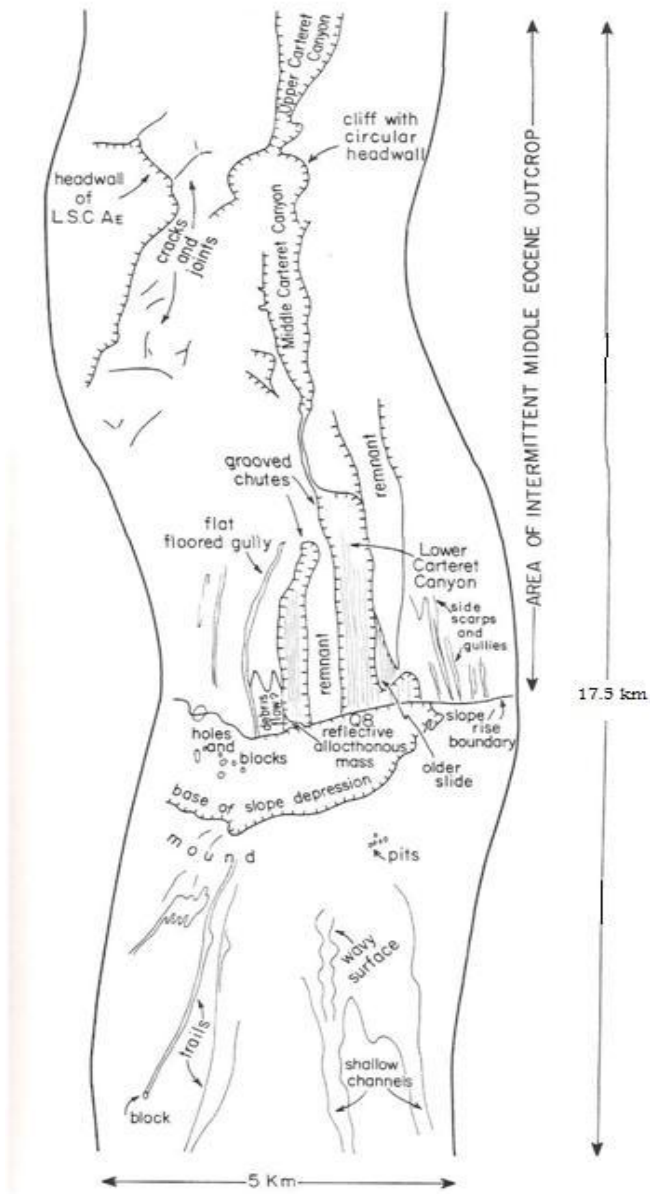


Figure 4b



Chicxulub Impact Melt Breccia Copyright © 2007 Calvin J. Hamilton

Figure 5



Figure 6

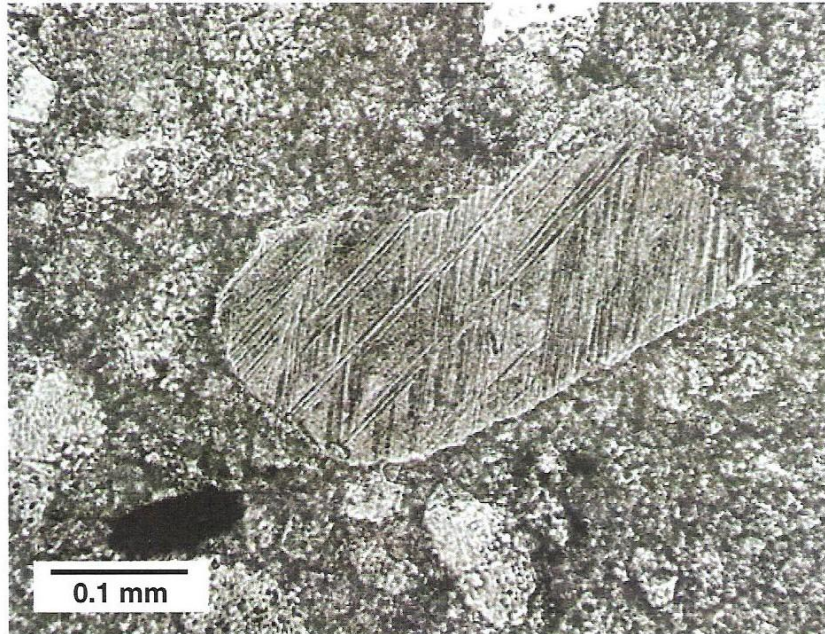


Fig. 4.19. Quartz; multiple PDFs, fresh. Shocked quartz grain containing multiple sets of fresh PDFs. The grain is included with rare sandstone fragments in a carbonate breccia dike that cuts the deformed basement rocks at Sierra Madera (Texas), an impact structure developed in a target composed dominantly of carbonate rocks. The closely spaced PDFs give a distinctive darkened, yellowish appearance to the quartz grain. Sample SMF-65-2-2 (plane-polarized light).

Figure 7a

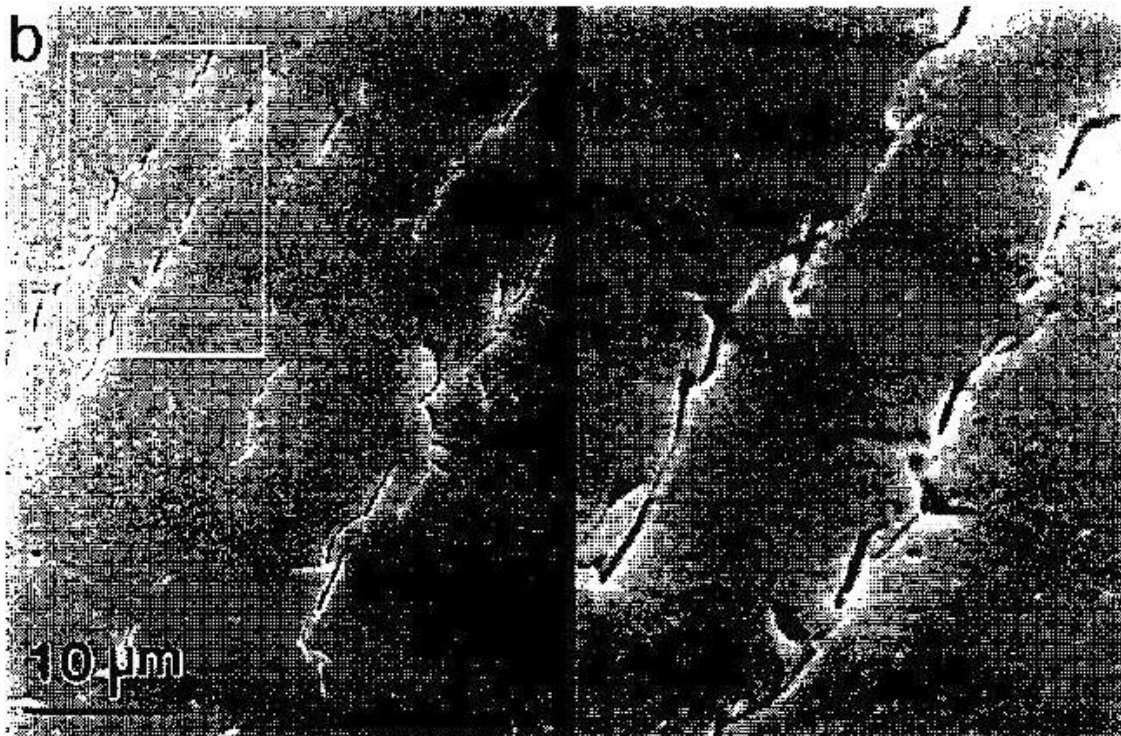


Figure 7b



Figure 8

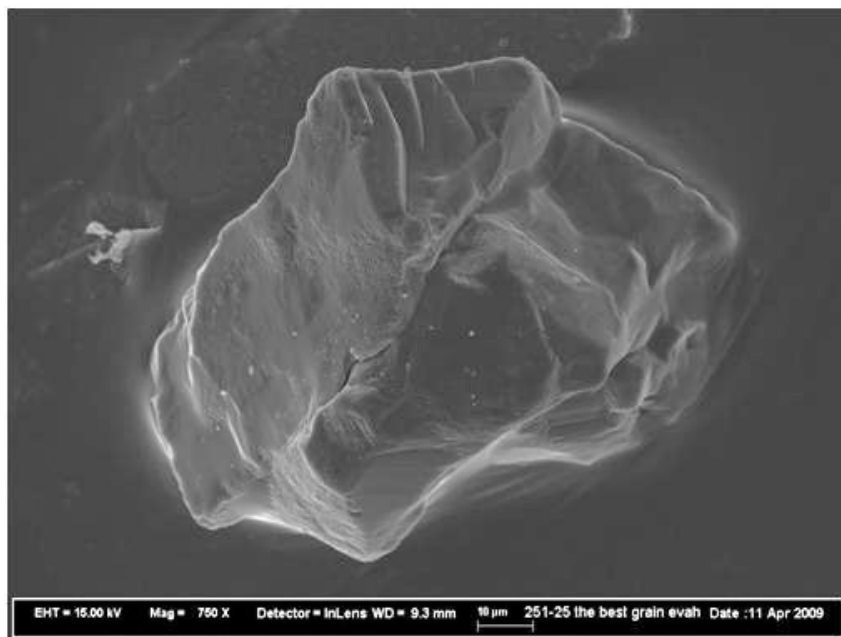


Figure 9a.1

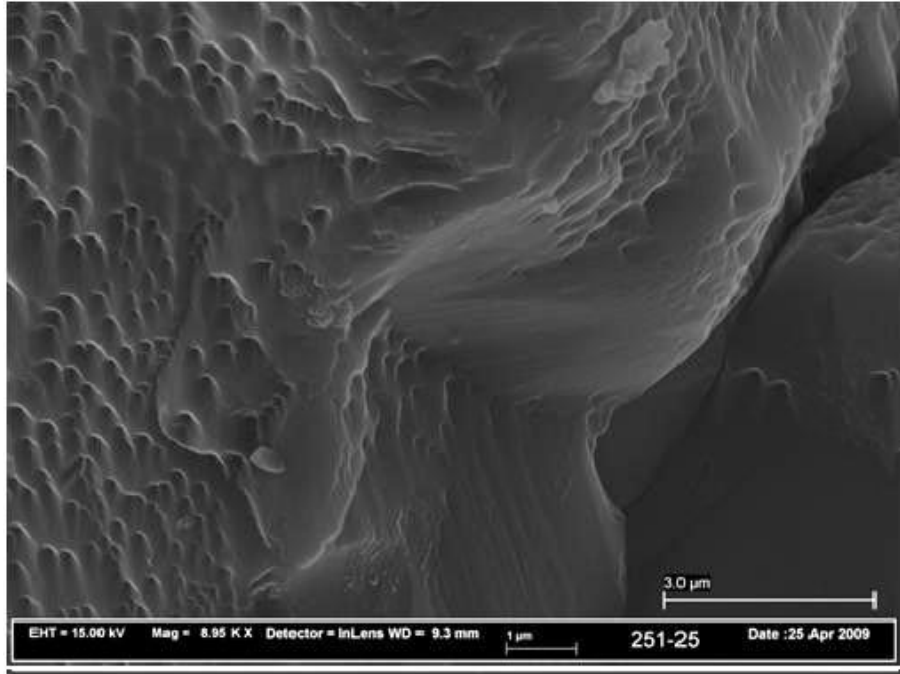


Figure 9a.2

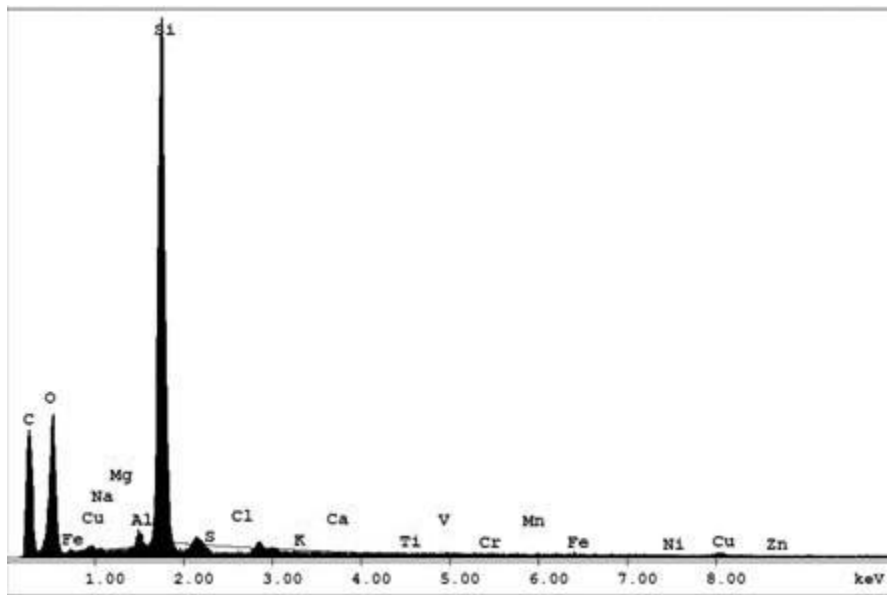


Figure 9a.3

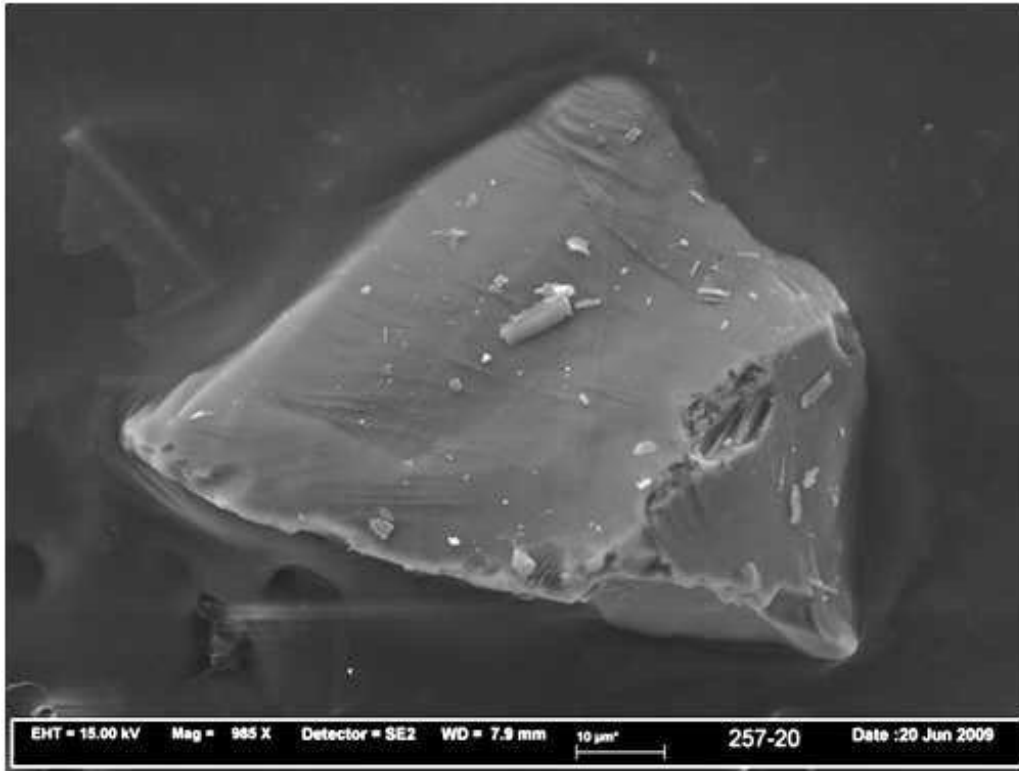
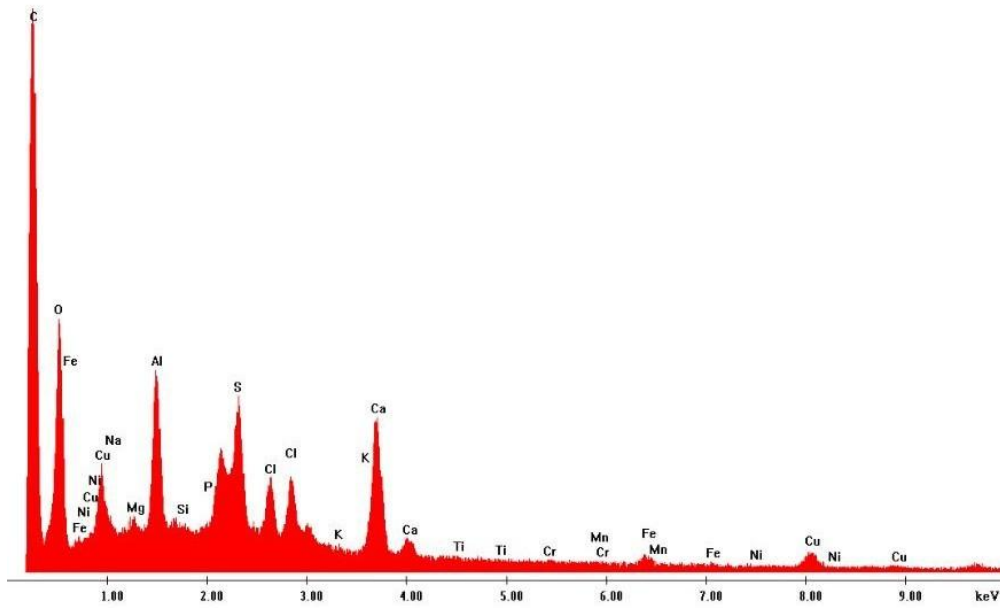


Figure 9b.1

Label A: 257-10a



9b.2

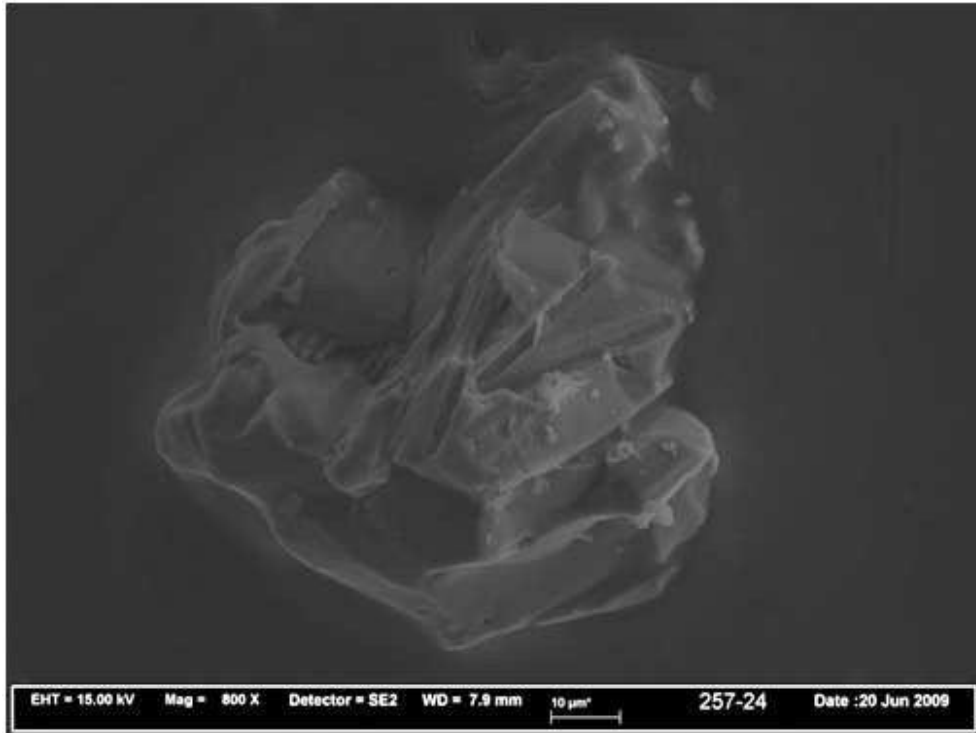


Figure 9c.1

Label A: 257-24a

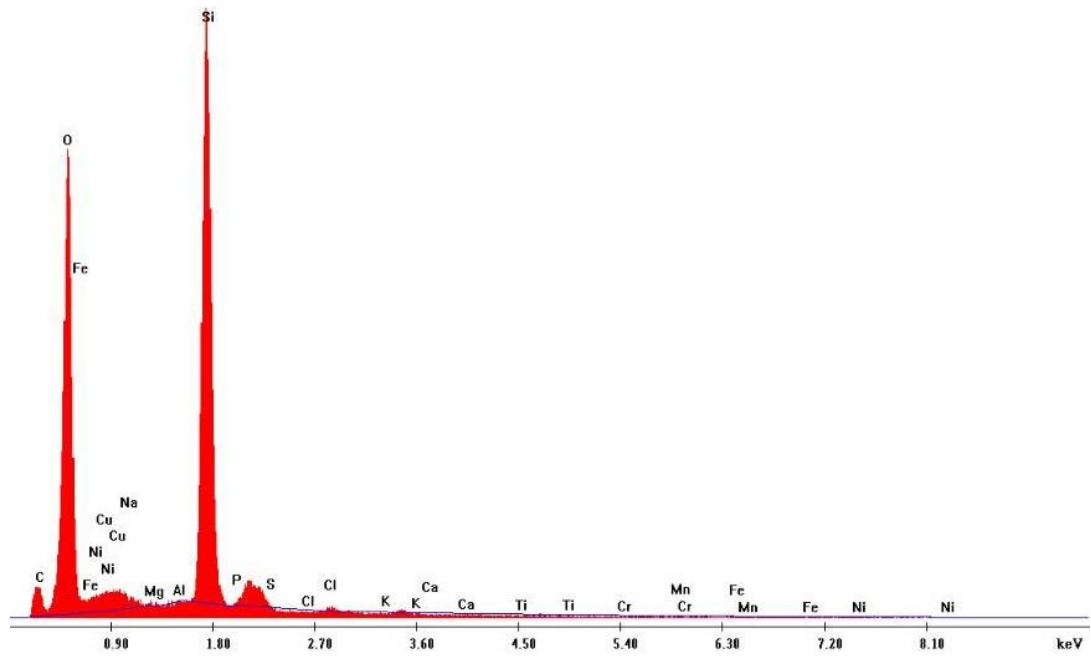


Figure 9c.2

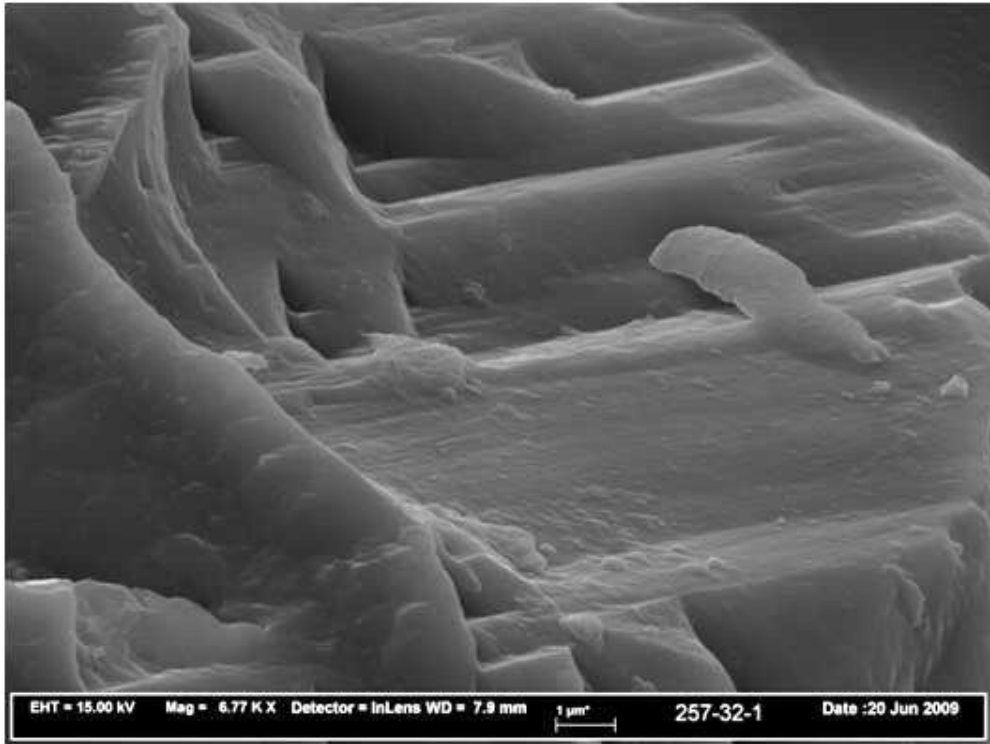


Figure 10a

Label A: 257-32a

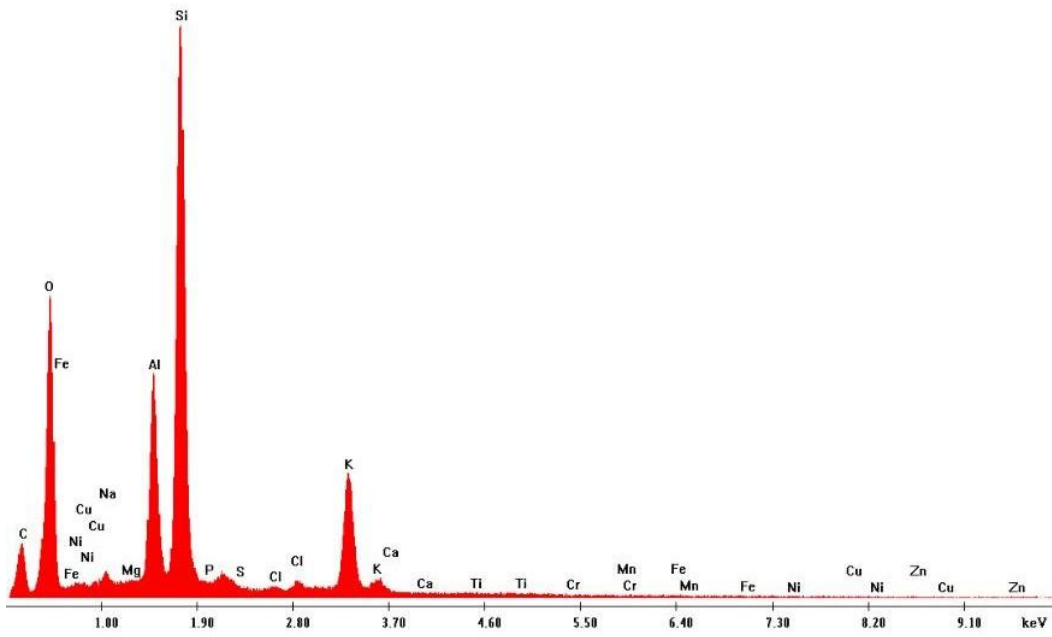


Figure 10b

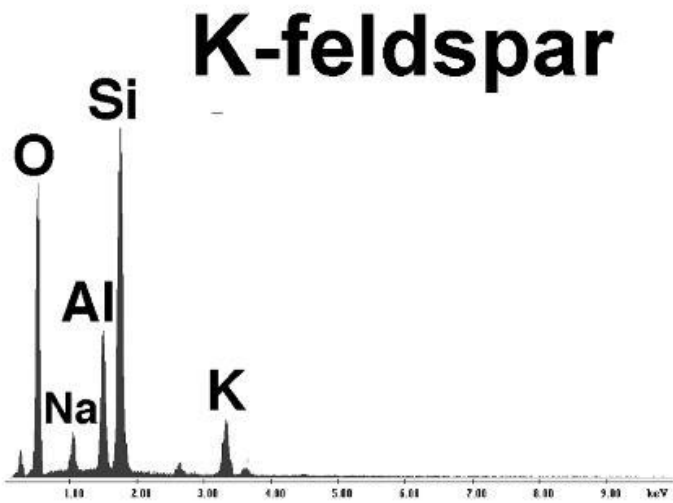
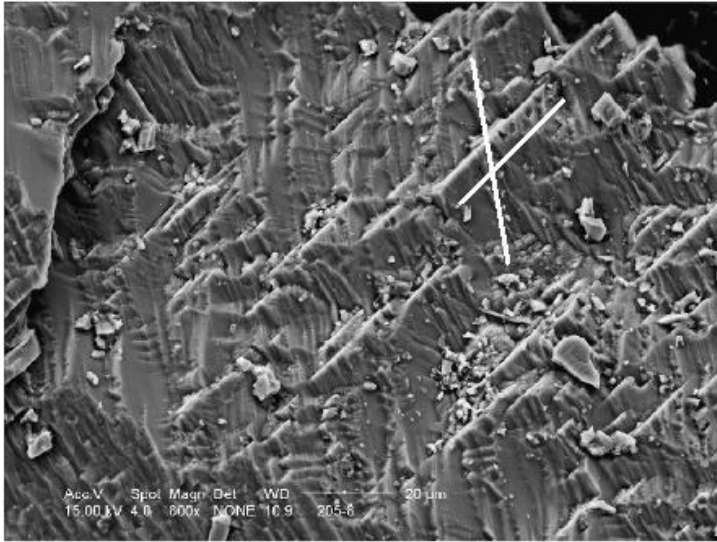


Figure 10c

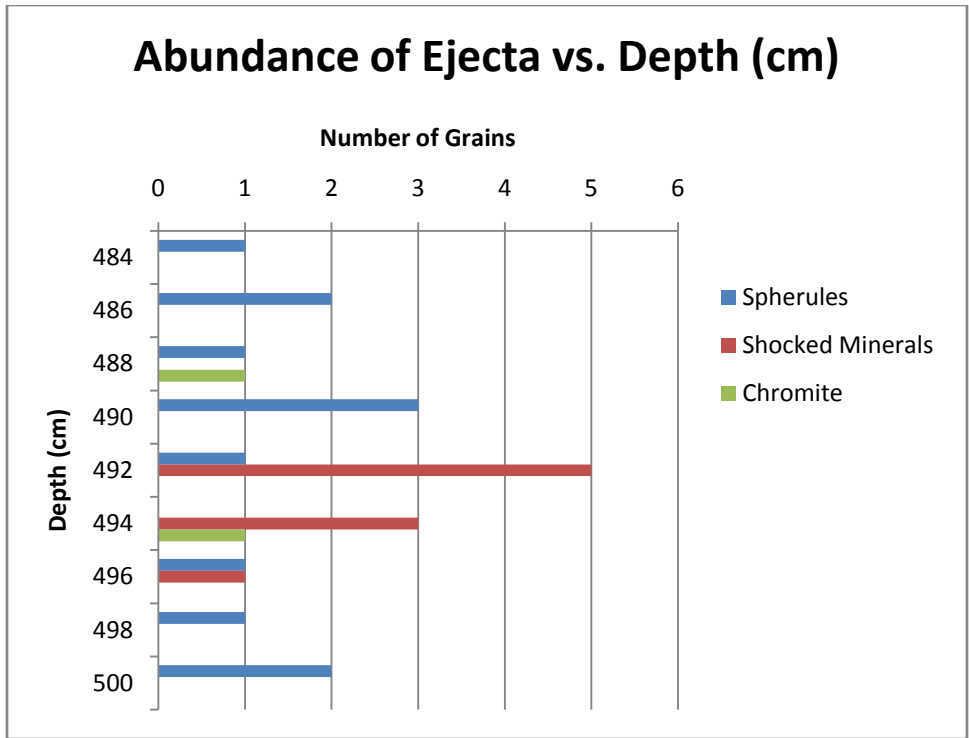


Figure 11

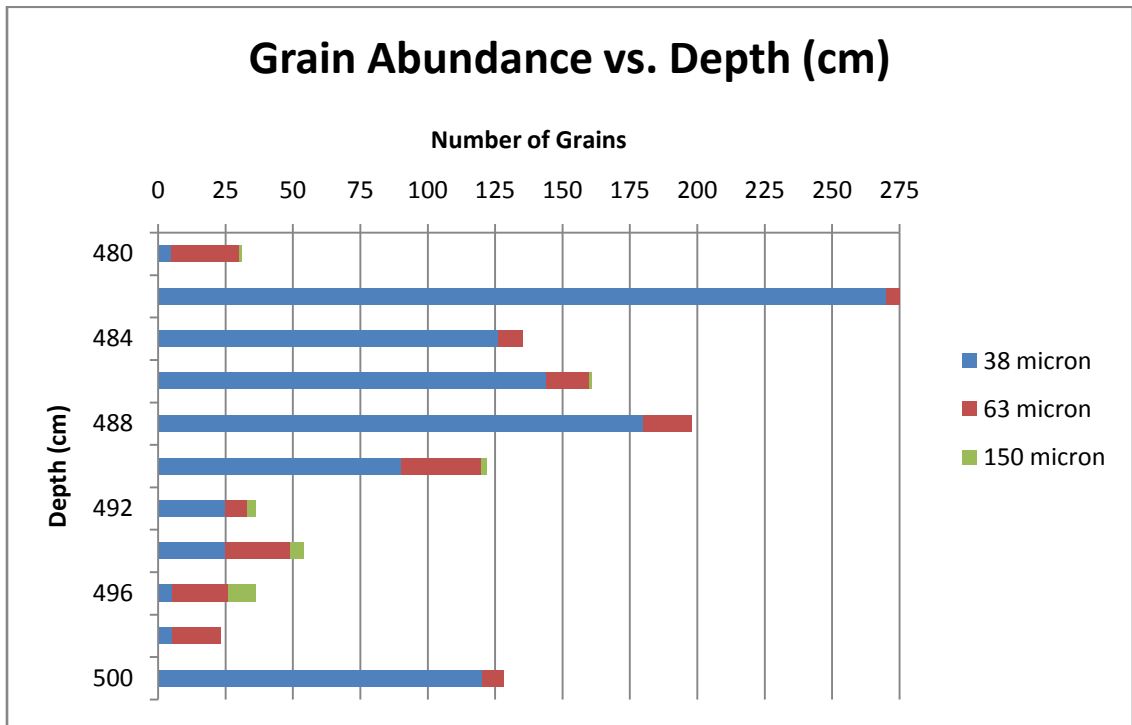


Figure 12

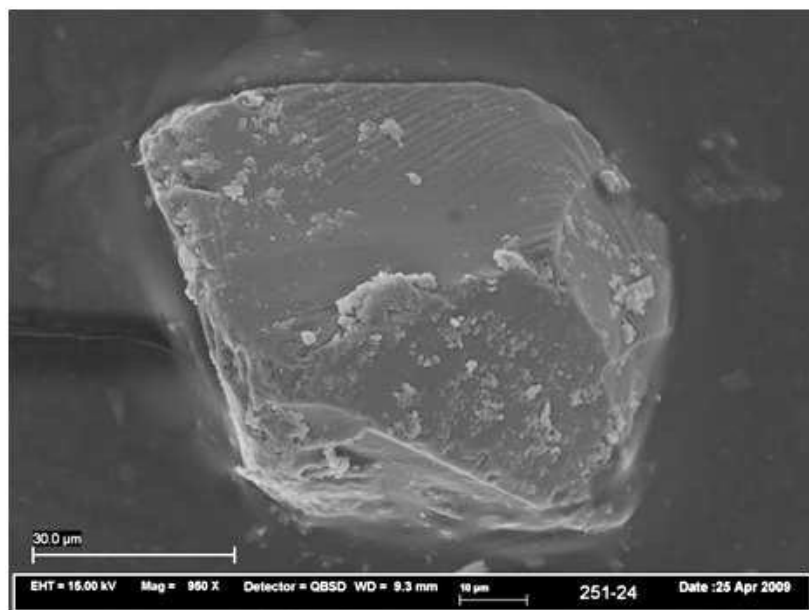


Figure 13a.1

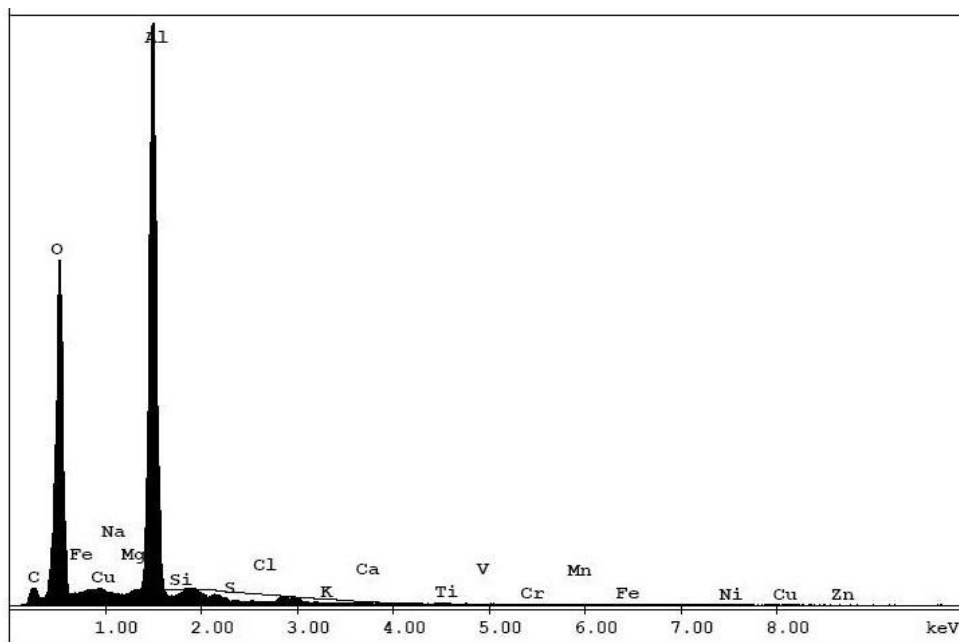


Figure 13a.2

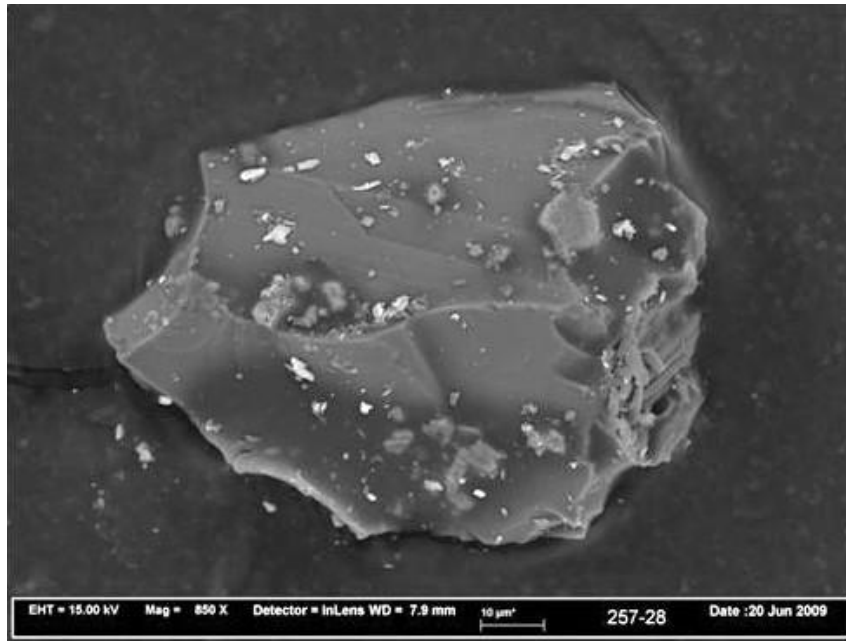


Figure 13b.1

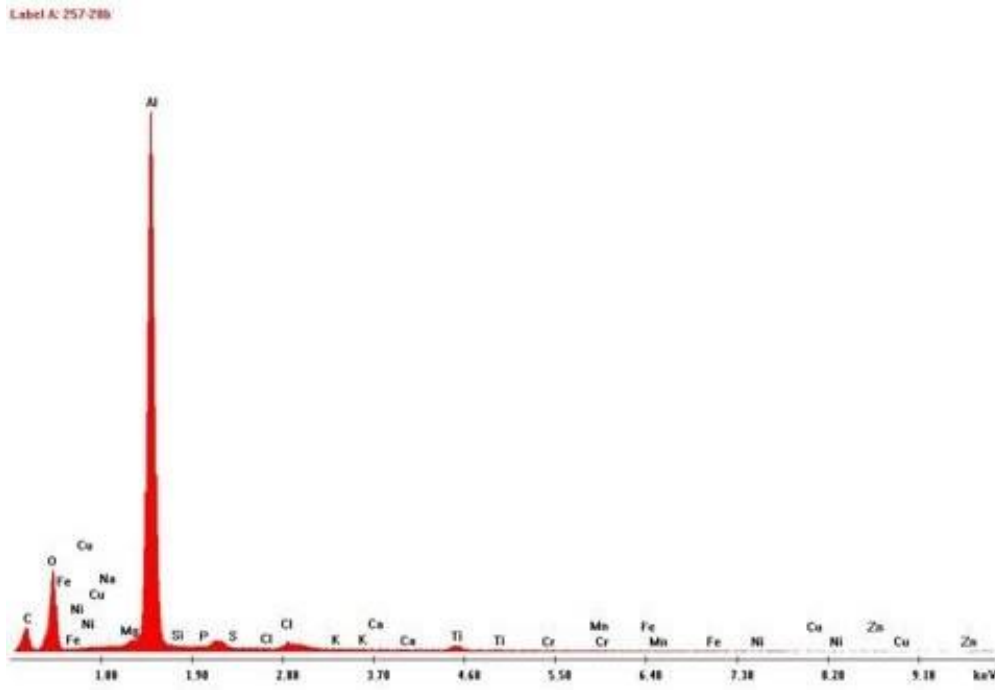


Figure 13b.2

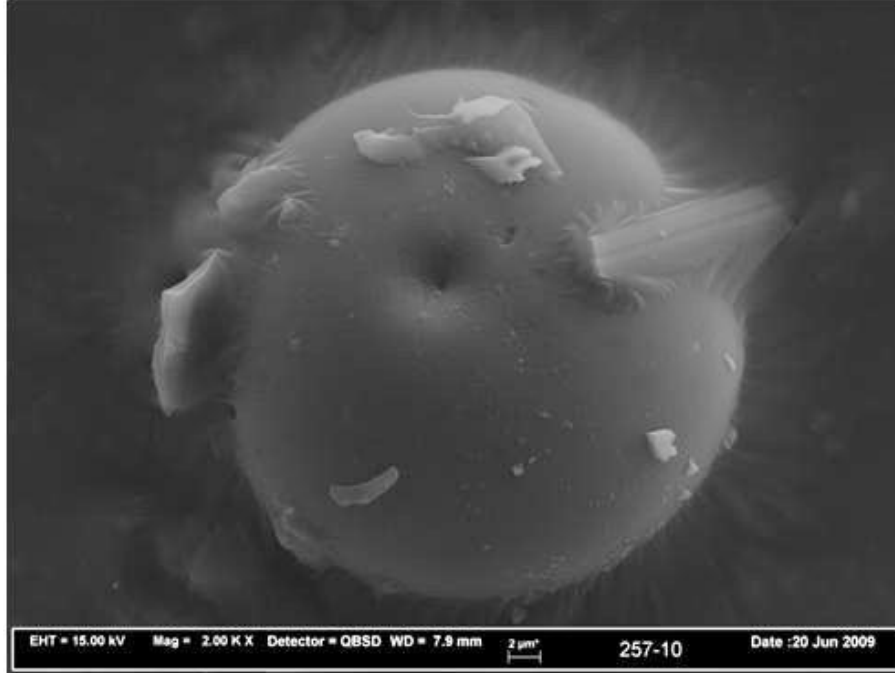


Figure 14a

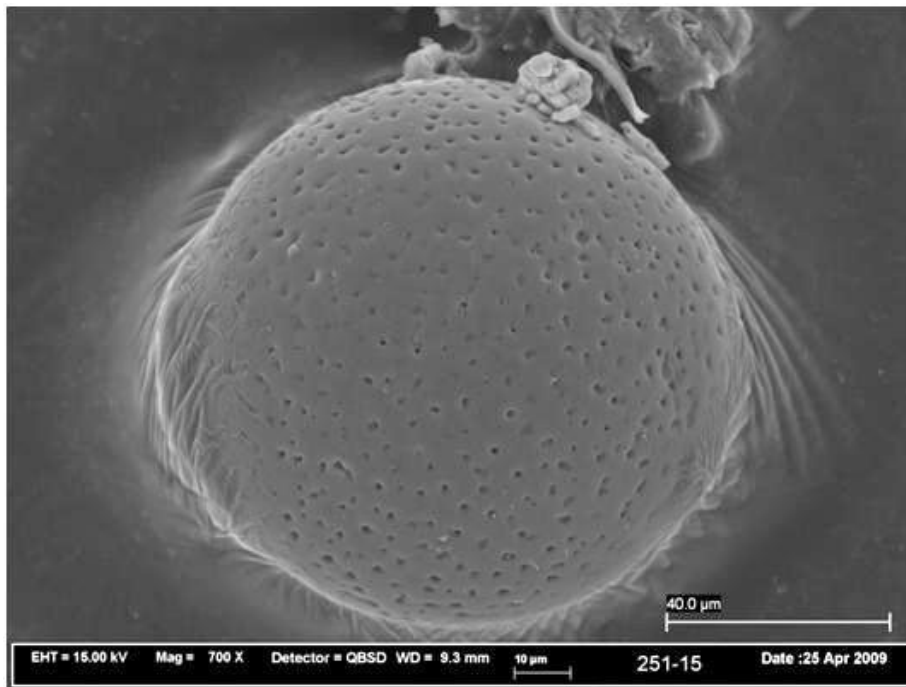


Figure 14b

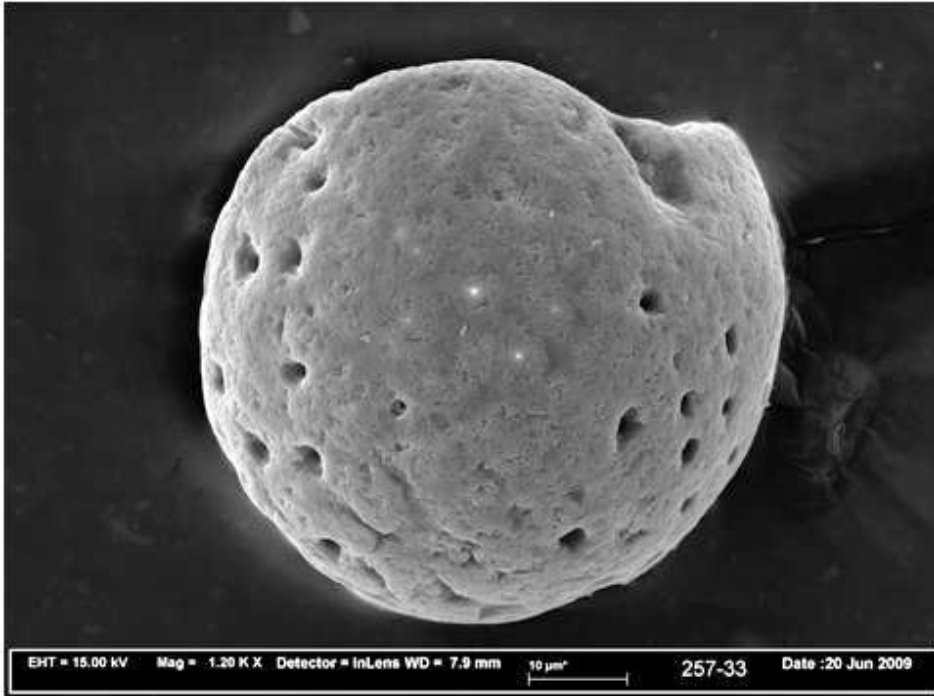


Figure 15a

Label A: 257-33a

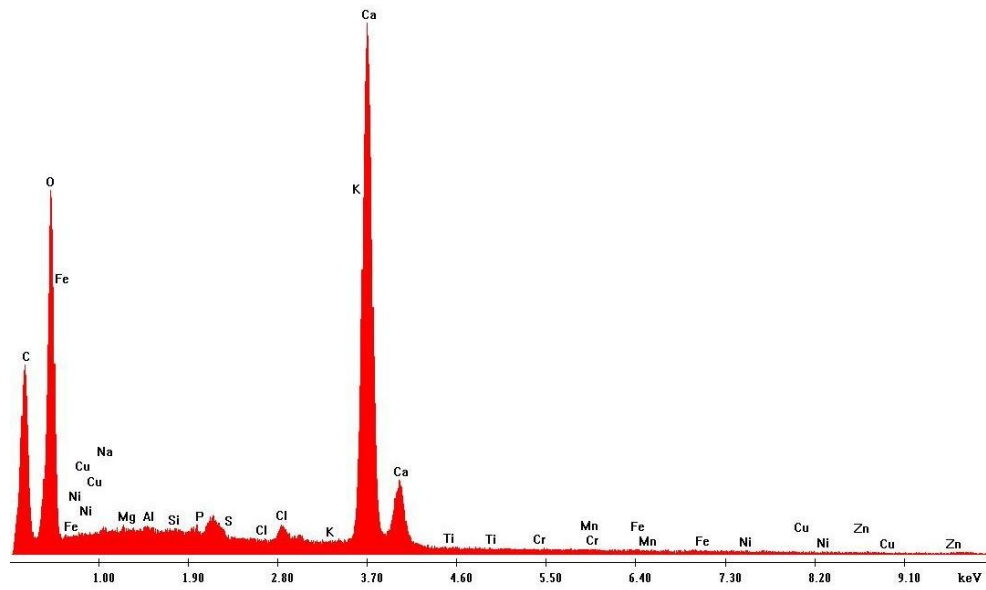


Figure 15b

Average Ejecta Thickness vs. Distance

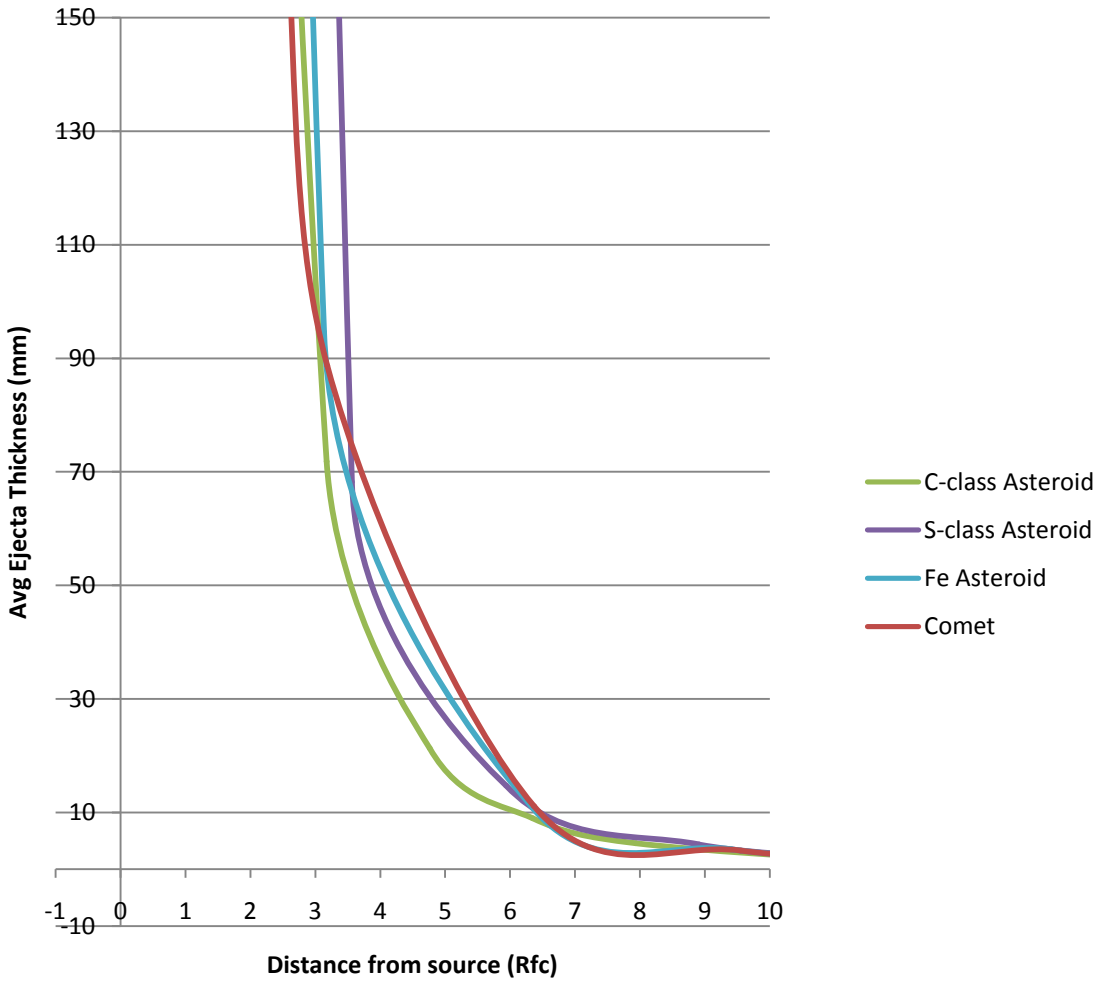


Figure 16

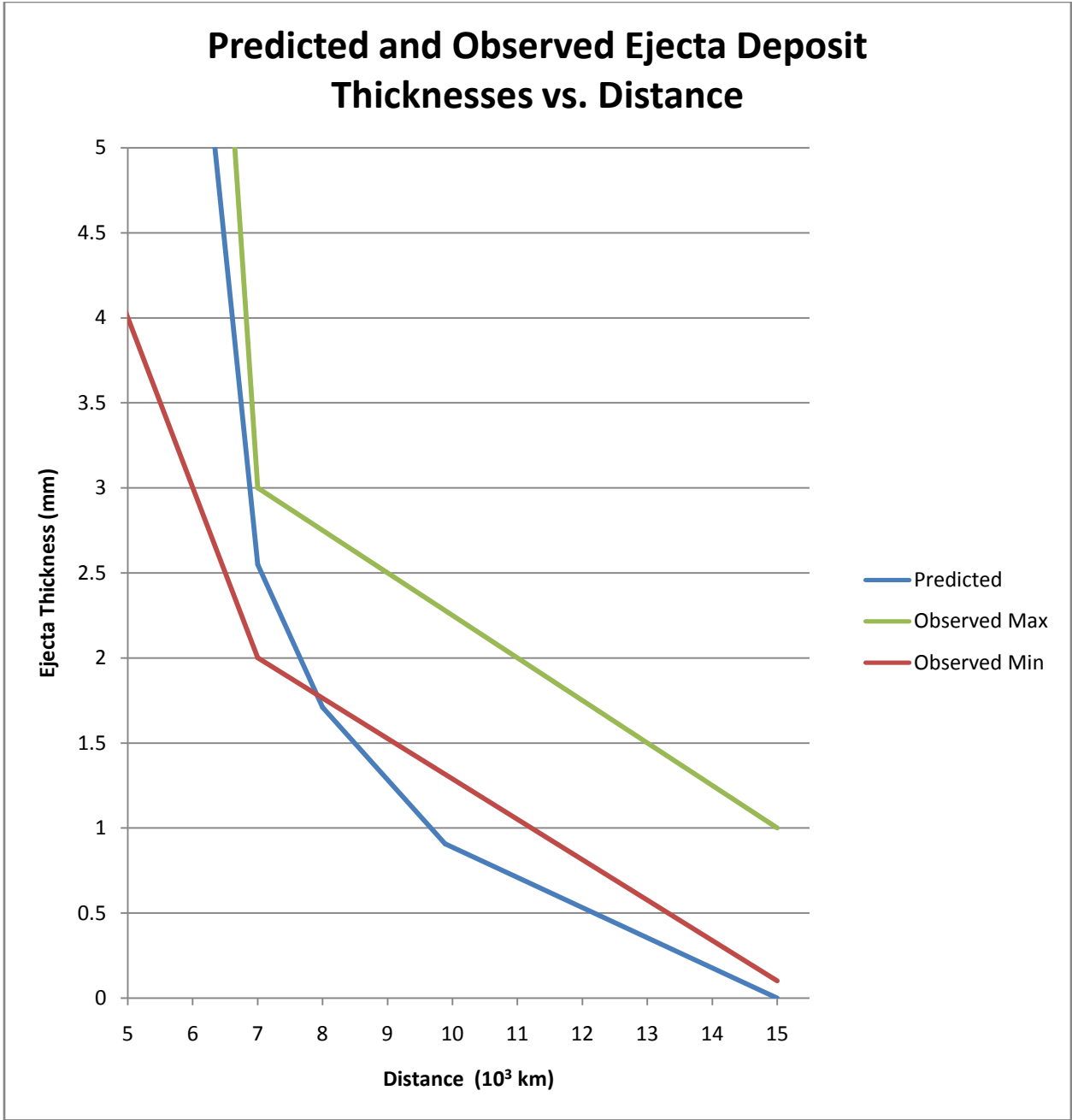


Figure 17

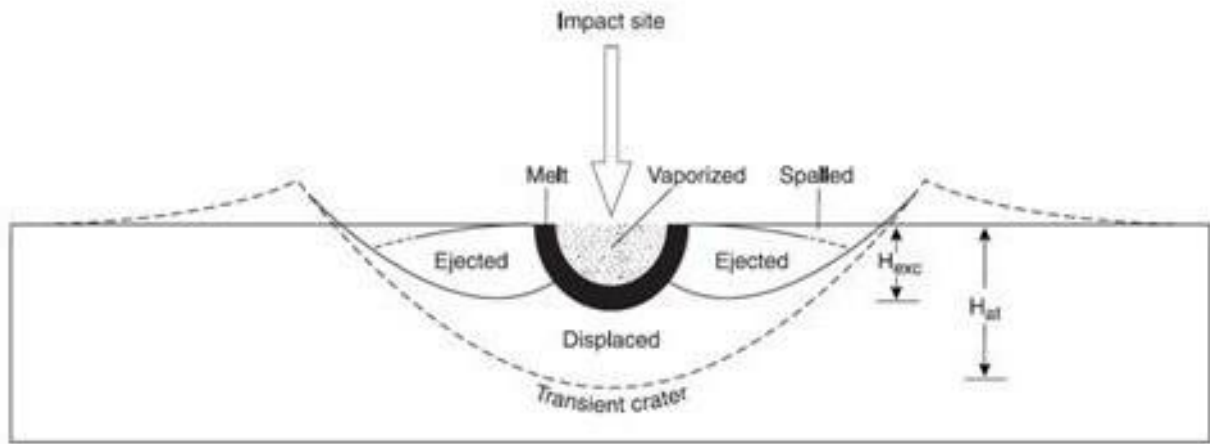


Figure 18

List of Tables

Table 1: Conditions of shock metamorphism compared to normal tectonic (regional and contact) metamorphism. From French, 1998.

Table 2: Correlation of shock pressures and temperatures to shock metamorphic effects, such as PDFs. From French, 1998.

Table 3: Typical angles between c-axis and angle normal to PDF orientation. From French, 1998.

Table 4: Table of prospective shocked grains and spherules recovered from Tamarack pond. Asterisks indicate no measurements taken.

Table 5: Atomic weight compositions and elemental ratios of Al-O grains recovered from Tamarack Pond.

Table 6: AMS C-14 dates from present study. All dates courtesy of the Lawrence Livermore National Laboratory's Center of Accelerated Mass Spectrometry.

Table 7: Inputs of size, density, speed, and impact angle for different impactors into Collins et al. 2005 computer model to recreate the dimensions of the crater candidate in Carteret Canyon. Crater depth~100m; Crater diameter~860m; Target density~1000 kg/m³; Water depth~1800m.

Table 8: Outputs from Collins et al. 2005 computer model for different impactors, keeping ejecta layer constant at 6 cm. Carteret Canyon depression volume ~3 km³.

Table 9: Thickness of discrete layer ejecta layer.

Tables

Characteristic	Regional and Contact Metamorphism; Igneous Petrogenesis	Shock Metamorphism
Geological setting	Widespread horizontal and vertical regions of Earth's crust, typically to depths of 10–50 km	Surface or near-surface regions of Earth's crust
Pressures	Typically <1–3 GPa	100–400 GPa near impact point; 10–60 GPa in large volumes of surrounding rock
Temperatures	Generally $\pm 1000^\circ\text{C}$	Up to 10,000°C near impact point (vaporization); typically from 500° to 3000°C in much of surrounding rock
Strain rates	$10^{-3}/\text{s}$ to $10^{-6}/\text{s}$	$10^4/\text{s}$ to $10^6/\text{s}$
Time for completion of process	From 10^5 – 10^7 yr	"Instantaneous": Shock-wave passage through 10-cm distance, $<10^{-5}$ s; formation of large (100-km-diameter) structure <1 hr
Reaction times	Slow; minerals closely approach equilibrium	Rapid; abundant quenching and preservation of metastable minerals and glasses

Table 1

Approximate Shock Pressure (GPa)	Estimated Postshock Temperature ($^\circ\text{C}$)*	Effects
2–6	<100	Rock fracturing; breccia formation Shatter cones
5–7	100	Mineral fracturing: (0001) and { in quartz
8–10	100	Basal Brazil twins (0001)
10	100*	Quartz with PDFs {10 $\bar{1}$ 3}
12–15	150	Quartz \rightarrow stishovite
13	150	Graphite \rightarrow cubic diamond
20	170*	Quartz with PDFs {10 $\bar{1}$ 2}, etc. Quartz, feldspar with reduced ref indexes, lowered birefringence
>30	275	Quartz \rightarrow coesite
35	300	Diaplectic quartz, feldspar glasses
45	900	Normal (melted) feldspar glass (v
60	>1500	Rock glasses, crystallized melt roc from liquids)
80–100	>2500	Rock glasses (condensed from vap

*For dense nonporous rocks. For porous rocks (e.g., sandstones), postshock temperatures (P = 10 GPa) and 1560°C (P = 20 GPa). Data from *Stöffler* (1984), Table 3; *Stöffler and Langenhorst* (1994), Table 8, p. 175.

Table 2

Symbol	Miller Indexes	Polar Angle (Angle Between Pole to Plane and Quartz c-axis)
c	*(0001)	0°
ω, ω'	*{10 $\bar{1}$ 3}, {01 $\bar{1}$ 3}	23°
π, π'	*{10 $\bar{1}$ 2}, {01 $\bar{1}$ 2}	32°
r, z	*{10 $\bar{1}$ 1}, {01 $\bar{1}$ 1}	52°
m	{10 $\bar{1}$ 0}	90°
ξ	{11 $\bar{2}$ 2}, {2 $\bar{1}$ 1 $\bar{2}$ }	48°
s	{11 $\bar{2}$ 1}, {2 $\bar{1}$ 1 $\bar{1}$ }	66°
a	{11 $\bar{2}$ 0}, {2 $\bar{1}$ 1 $\bar{0}$ }	90°
t	*{22 $\bar{4}$ 1}, {42 $\bar{2}$ 1}	77°
k	{4041}, {0441}	79°
x	{51 $\bar{6}$ 0}, {6 $\bar{1}$ 50}	90°
—	{6 $\bar{1}$ 51}, {15 $\bar{6}$ 1}	82°
—	{3141}, {43 $\bar{1}$ 1}	78°
—	{4 $\bar{1}$ 31}, {1341}	74°
—	{21 $\bar{3}$ 1}, {32 $\bar{1}$ 1}	74°
—	{3 $\bar{1}$ 21}, {1231}	74°

*Prominent planes in typical shock fabrics.

Table 3

Grain #	Depth (cm)	Size fraction (μm)	Size (μm)	Mineral type	Shock lamellae	# of Directions	Spacing
257-38	488-490	38	60	Cr-spinel	*	*	*
251-24	492-494	63	70	Al-O	yes	2+	9nm
251-25	492-494	63	70	quartz	yes	3+	.2μm
251-27	492-494	63	70	quartz	yes	3+	1μm
257-28	492-494	38	60	Al-O	yes	2+	2μm
257-32	492-494	38	*	K-spar	yes	1+	38nm
253-23	494-496	63	*	quartz	yes	3+	*
253-27	494-496	63	*	K-spar	*	*	*
257-24	494-496	38	60	quartz	yes	3+	1nm
257-25	494-496	38	*	Cr-spinel	yes?	1	.5μm
257-20	496-498	38	60	quartz	yes	2+	1μm

Spherules

Grain #	Depth (cm)	Size Frac (μm)	Diameter (μm)	Composition (EDX)	Description/Color
257-47	484-486	38	40.28	C	vitreous black spherule, possible ablation tracks, crater
251-36	486-488	63	4, 2.8	C	two C-rich spherules on white plagioclase feldspar, smooth texture
252-7	488-490	38	40	C	vitreous, black, smooth C spherule
252-5	490-492	38	*	C	clear, broken C spherule
252-2	490-492	38	52	C	vitreous, red, broken C spherule with minor O
257-37	490-492	38	35.8	C	clear, smooth spherule with possible quench texture
251-15	490-492	63	98	C	vesicular carbon spherule with minor O peak, pitted surface
257-33	492-494	38	59.55	CaCO3	clear spherule, possibly shocked, triangles may indicate Brazil twinning
257-19	496-498	38	40.7 x 33.3	C	smooth black surface, Ca and Al peak
257-17	498-500	38	24	C	smooth black surface, Ca, Al
257-7	500-502	38	35.7	C	vitreous, black, nearly pure C spherule, small O peak
257-10	500-502	38	34.6	C	black spherule, smooth

Table 4

Grain #	Depth (cm)	Size (μm)	C	Al	O	Ca	Si	S	Total	Si:O	Si:Al
251-36	486-488	63	6.42	10.61	50.07	1.28	24.52	0	92.9	0.489714	2.311027
252-11	488-490	38	66.16	8.05	16.76	0	8.6	0.07	99.64	0.513126	1.068323
252-17	488-490	63	61.73	16.51	19.61	0	0	0	97.85	0	0
250-37	488-490	150	62.42	0.9	31.57	0.51	0.09	0.84	96.33	0.002851	0.1
251-10	490-492	63	91.23	2.75	5.63	0	0.14	0.01	99.76	0.024867	0.050909
251-14	490-492	63	74.19	0.22	22.81	0.06	0.09	0.34	97.71	0.003946	0.409091
252-2	490-492	38	70.26	0.45	25.38	0.33	0.06	0.3	96.78	0.002364	0.133333
251-24	492-494	63	9.17	35.37	54.91	0	0	0	99.45	0	0
257-28	492-494	38	17.62	33.96	47.84	0	0.16	0	99.58	0.003344	0.004711
257-30	492-494	38	25.29	41.93	22.22	0	0	0.11	89.55	0	0
253-25	494-496	63	60.48	1.4	31.63	0.46	0.06	0.91	94.94	0.001897	0.042857
253-26	494-496	63	61.81	1.89	26.49	1.03	0.03	1.09	92.34	0.001133	0.015873

Si:O	Si:Al	C:Al	C:O	Al:O
			0.12822	
0.489714	2.311027	0.60509		0.211903
			3.947494	
0.513126	1.068323	8.218634		0.48031
			3.147884	
0	0	3.738946		0.841917
			1.977194	
0.002851	0.1	69.35556		0.028508
			16.20426	
0.024867	0.050909	33.17455		0.488455
			3.252521	
0.003946	0.409091	337.2273		0.009645
			2.768322	
0.002364	0.133333	156.1333		0.01773
			0.167001	
0	0	0.259259		0.644145
			0.368311	
0.003344	0.004711	0.518846		0.709866
			1.138164	
0	0	0.603148		1.887039
			1.912109	
0.001897	0.042857	43.2		0.044262
			2.333333	
0.001133	0.015873	32.7037		0.071348

Table 5

Sample Name	$\delta^{13}\text{C}$	Fraction Modern	\pm	D^{14}C	\pm	^{14}C age	\pm	Calendar Age	\pm
TP 500-502	-25	0.7503	0.0031	-249.7	3.1	2310	35	2350	10

1) $\delta^{13}\text{C}$ values are the assumed values according to Stuiver and Polach (Radiocarbon, v. 19, p.355, 1977) when given without decimal places. Values measured for the material itself are given with a single decimal place.

2) The quoted age is in radiocarbon years using the Libby half life of 5568 years and following the conventions of Stuiver and Polach (ibid.).

3) Radiocarbon concentration is given as fraction Modern, D^{14}C , and conventional radiocarbon age.

4) Sample preparation backgrounds have been subtracted, based on measurements of samples of ^{14}C -free coal.

5) Radiocarbon ages courtesy of the Lawrence Livermore National Laboratory—Center for Accelerator Mass Spectrometry. Calendar ages were derived from the IntCal04 Terrestrial Radiocarbon Age Calibration curve (Reimer et al., 2004).

Table 6

Type	Density (kg/m^3)	Diameter (m)	Speed (km/s)	Angle (deg.)	Final Crater Diameter (m)	Final Crater Depth (m)	End of Ejecta Layer (km)
Comet	1000	745.93	51	45	785	167	111.25
C-class Asteroid	1500	589.5	17	45	630	134	83
S-Class Asteroid	3000	285	17	45	674	238	122
Iron-rich Asteroid	8000	125	17	45	797	170	113

Table 7

Constraining Impact Melt Volume and Distribution from Ejecta Layer Thickness (with Collins et al. 2005 computational model)							
Density (km ³)	Size (m)	Speed (km/s)	Thickness of Ejecta Layer (cm)	Final Crater Radius (km)	Final Crater Depth (km)	Volume of Melt (km ³)	Visible Fireball Radius (km)
1000	3650	51	6.07	31.7	0.838	32.9	56.5
1500	4475	17	5.97	31.6	0.837	23.5	35.7
3000	3085	17	6.01	31.6	0.837	20.3	30.0
8000	1875	17	6.00	31.6	0.837	16.0	242.2

Table 8

Depth (cm)	>38 μm	>63 μm	>150 μm
492-494	3	8	25
494-496	5	24	25
496-498	12	13	5
Total Grains	20	45	55
Area(sq. μm)	3000	2835	2090

Lithic Area (sq. μm)	7925
Total Area (sq. μm)	400,000,000
Thickness (μm)	1.98125 x 10 ⁻⁵

Table 9

Appendix I

Grain #	Core	Depth cm	Size	Initial Description	SEM analysis
250-34	TP1	488-490	>150	triangular black grain	melting C rich grain
250-35	TP1	488-490	>150	white grain	mungy grain
250-36	TP1	488-490	>150	black grain	sediment fossil cast? (C-rich material with minor Ca, Al and Cl)-minor Cu- fossil before it
250-37	TP1	488-490	>150	black semi-round grain	turned to glauconite) fibrous texture on possible melted
250-38	TP1	488-490	>150	metal splash on white grain	sediment fibrous texture on possible melted
250-39	TP1	488-490	>150	metal splash on white grain	sediment
250-40	TP1	488-490	>150	metal splash on white grain	carbonate coating on organic material
250-41	TP1	488-490	>150	white spheroid	membrane sensitive to beam
250-42	TP1	488-490	>150	white and brown grain	vesicular-sensitive to beam
250-43	TP1	488-490	>150	shiny vesicular brown grain	sensitive to beam
250-44	TP1	488-490	>150	marine organic material	organic C
250-45	TP1	488-490	>150	in glue	
250-46	TP1	488-490	>150	brown glass with metal splash	mungy C grain
250-47	TP1	488-490	>150	brown glass with metal splash	mungy C grain carbon spherule with passenger spherule on top of C rich fossil cast with minor Cu?)
250-48	TP1	488-490	>150	black spheroid	-where does the S come from? OR organic matter
250-49	TP1	488-490	>150	black spheroid	covered with glue
250-50	TP1	488-490	>150	black spheroid	organic microfossil cast with adsorbed Cu
250-51	TP1	488-490	>150	black spheroid	organic microfossil cast with adsorbed Cu
250-52	TP1	488-490	>150	black spheroid	organic microfossil cast with adsorbed Cu
250-53	TP1	488-490	>150	black spheroid	organic microfossil cast with adsorbed Cu
250-54	TP1	488-490	>150	black grain with white on top	concoiddally fractured pure SiO2 glass
250-55	TP1	488-490	>150	white grain	buried in glue calcium carbonate with organic matter enriched in Cu in the middle
250-56	TP1	488-490	>150		
250-57	TP1	488-490	>150	black ovoid	vesicular C microfossil cast enriched in Cu
250-58	TP1	488-490	>150	black spheroid	vesicular C microfossil cast enriched in Cu
251-1	TP1	490-492	>150	black spheroid	vesicular organic C rich microfossil cast
251-2	TP1	490-492	>150	organic C	
251-3	TP1	490-492	>150	black spheroid	vesicular organic C rich microfossil cast
251-4	TP1	490-492	>150	black spheroid	vesicular organic C rich microfossil cast
251-5	TP1	490-492	>150	melted sediment	
251-6	TP1	490-492	>150	black glassy grain	carbon with minor Ca
251-7	TP1	490-492	>150	black tear drop shaped grain	in glue
251-8	TP1	490-492	>150	textured organic C rich sediment	

				cm	
251-9	TP1	490-492	>150	white grain with odd shape	shocked carbon? with 16 nm spacing of lamellae and three directions of lamellae
251-10	TP1	490-492	>63	C with minor Al peak	
251-11	TP1	490-492	>63	glassy black grain	sediment with glass with bulbous surface
251-12	TP1	490-492	>63	carbon glass	
251-13	TP1	490-492	>63	sedimentary aggregate	
251-14	TP1	490-492	>63	C with minor O peak	
251-15	TP1	490-492	>63	dark reddish brown spherule	vesicular carbon spherule with minor O peak
251-16	TP1	490-492	>63	diatom trap	
251-23	TP1	492-494	>63u	marine spine	carbon spine
251-24	TP1	492-494	>63u		aluminum oxide with lamellae 9 nm apart -shocked kaolinite or shocked corundum? shocked quartz with aerodynamic ablation of pdfs plus spherule with passenger spherule plus interference pattern of pdfs plus aluminosilicate (sillimanite?) (minor Cu peak)
251-25	TP1	492-494	>63u	clear vesicular grain	
251-26	TP1	492-494	>63u	in the glue-possible glass	
251-27	TP1	492-494	>63u	clear to white grain	shocked quartz being melted with organic coating on some pdfs
251-28	TP1	492-494	>63u	black grain	vesicular organic rich material
251-29	TP1	492-494	>63u	brown grain	organic stuff
251-30	TP1	492-494	>63u	black ovoid	vesicular organic rich material
251-31	TP1	486-488	>63u	white spherule	CaCO ₃ spherule-not perfectly round
251-32	TP1	486-488	>63u	black glassy ovoid	Si-C rich glass with Mn, Fe, Ca, Ti
251-33	TP1	486-488	>63u	white milky grain	SiO ₂
251-34	TP1	486-488	>63u	black fossil shaped grain	vesicular organic rich material
251-35	TP1	486-488	>63u	black ovoid	vesicular organic rich material
251-36	TP1	486-488	>63u	white milky grain	two spherules on Na rich plagioclase feldspar with Al silicate material (glass?)
251-37	TP1	486-488	>63u	gray grain	mungy sediment
251-38	TP1	486-488	>63u	black grain	organic stuff
251-39	TP1	486-488	>63u	gray grain with black inclusion	mungy sediment
251-40	TP1	486-488	>63u	metallic grain	grain with lines-sensitive to beam
252-2	TP1	490-492	>38u	shiny reddish brown spherule	broken C spherule with minor O, some Cu contamination
252-3	TP1	490-492	>38u	disc shaped silicate fossil	detrital grain
252-4	TP1	490-492	>38u	organic C	
252-5	TP1	490-492	>38u	broken C spherule	
252-6	TP1	490-492	>38u	vesicular organic C with some Cu contamination	
252-7	TP1	488-490	>38u	round, black glassy grain	smooth C spherule with some Cu contamination

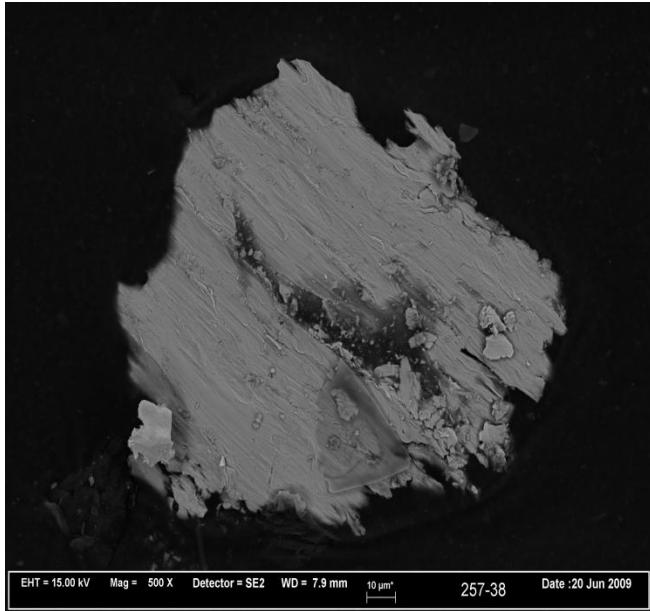
252-8	TP1	488-490	>38u	round, black glassy grain	organic C with some Cu contamination
252-9	TP1	488-490	>38u	round, black glassy grain	organic C with some Cu contamination
252-10	TP1	488-490	>38u	long shiny black vitreous grain	organic C with some Cu contamination
252-11	TP1	488-490	>38u	semi-round gray grain	aluminosilicate with some C
252-12	TP1	488-490	>38u	round translucent white grain	pollen grain
252-13	TP1	488-490	>38u	gone	
252-14	TP1	488-490	>63u	SiO2-not shocked	
252-15	TP1	488-490	>63u	blue wormy thing	organic stuff
252-16	TP1	488-490	>63u	gold possibly biogenic grain	organic stuff
252-17	TP1	488-490	>63u		Al oxide with C and Cu contamination
252-18	TP1	488-490	>63u	organic stuff	
252-52	TP1	492-494	>38u	milky quartz grain	SiO2-not shocked
252-53	TP1	492-494	>38u	gold grain	to do
252-54	TP1	492-494	>38u	light brown and black grain	K-feldspar
252-55	TP1	492-494	>38u	carbonate with metal	to do
252-56	TP1	492-494	>38u	carbonate with metal	to do
252-57	TP1	492-494	>38u	red grain	
252-58	TP1	492-494	>38u	carbonate with metal	not there
252-59	TP1	492-494	>38u	carbonate with metal	
253-21	TP1	494-496	>63u	milky white grain	foram fragment with well preserved coccolith on surface
253-22	TP1	494-496	>63u	clear glass	nearly pure C with Cl, Na, K, Ca peaks
253-23	TP1	494-496	>63u	milky white grain	SiO2-probably shocked in 3 directions
253-24	TP1	494-496	>63u	milky white grain	K-feldspar-nearly pure
253-25	TP1	494-496	>63u		nearly pure C with Al, Ca, Cu peaks
253-26	TP1	494-496	>63u	*	nearly pure vesicular C with Al, Ca, Cu peaks
253-27	TP1	494-496	>63u	clear glass	K-feldspar-nearly pure-has cleavage
253-28	TP1	482-484	>38u	black glassy spherule?	
253-29	TP1	482-484	>38u	milky white grain	
253-30	TP1	482-484	>38u	clear glass	
253-31	TP1	482-484	>38u	translucent amber glass	
253-32	TP1	482-484	>38u	milky and clear grain	
253-33	TP1	482-484	>38u	milky and clear grain	
253-34	TP1	482-484	>38u	translucent amber glass	
253-35	TP1	482-484	>38u	translucent amber glass	
253-36	TP1	482-484	>38u	milky white grain	
253-37	TP1	482-484	>38u	milky white grain	
253-38	TP1	482-484	>63u	yellow fragment	
253-39	TP1	482-484	>63u	black glass	
253-40	TP1	482-484	>63u	milky white grain	
253-41	TP1	482-484	>63u	black glass	
253-42	TP1	482-484	>63u	milky white grain	
253-43	TP1	482-484	>63u	milky white grain	

253-44	TP1	482-484	>38u	clear glass	
253-45	TP1	482-484	>38u	milky white grain	
253-46	TP1	482-484	>38u	rounded black grain	
253-47	TP1	482-484	>38u	milky white grain	
253-48	TP1	482-484	>38u	black glass	
253-49	TP1	482-484	>38u	black glass	
257-5	TP1	500-502	>38u	missing	
257-6	TP1	500-502	>38u	possible shocked quartz	SiO2 sensitive to beam-triangles and boxes
257-7	TP1	500-502	>38u	spherule	
257-8	TP1	500-502	>38u	possible shocked quartz	C with Na and Cl peak-mungy
257-9	TP1	500-502	>38u	clear round possible spherule	pollen
257-10	TP1	500-502	>38u	Spherule	C spherule with smooth surface
257-11	TP1	500-502	>38u	organic matter	
257-12	TP1	500-502	>38u	possible shocked quartz	SiO2-curved fractures-not shocked
257-13	TP1	500-502	>38u	possible shocked quartz	SiO2-curved fractures-not shocked
257-14	TP1	500-502	>38u	possible shocked quartz	organic matter
257-15	TP1	498-500	>38u	possible shocked quartz	SiO2-mungy-not shocked
257-16	TP1	498-500	>38u	possible shocked quartz	mungy SiO2-not shocked
257-17	TP1	498-500	>38u	spherule	smooth C spherule with Ca, Al, Cu sensitive to beam
257-18	TP1	496-498	>38u	Spherule Spherule	organic C spherule with smooth surface, Ca and Al peak, no Cu
257-19	TP1	496-498	>38u		
257-20	TP1	496-498	>38u	possible shocked mineral	
257-22	TP1	494-496	>38u	organic	
257-23	TP1	494-496	>38u	sediment	
257-24	TP1	494-496	>38u	shocked quartz	
257-25	TP1	494-496	>38u	biotite (kinked?)	chromite
257-26	TP1	494-496	>38u	possible carbonate	organc C sediment, possibly glauconite,
257-27	TP1	494-496	>38u		aluminosilicate spherule? D=100nm
257-28	TP1	492-494	>38u	amber shard of glass	al oxide lamellae in at least 2 directions
257-29	TP1	492-494	>38u	clear possible shocked quartz	organic
257-30	TP1	492-494	>38u	dark lithic fragment	Al oxide with Cu sediment
257-31	TP1	492-494	>38u	carbonate composite	Al oxide with Cu sediment
				White grain	K-spar, some parts with and w/o cleavage; strange diamond feature, cleave at 120 deg, not 90 deg, lamellae@ 32nm
257-32	TP1	492-494	>38u	White grain	CaCO3, triangles possibly indicating Brazil twinning, D=59.55 micron, submicron lamellae,=foram
257-33	TP1	492-494	>38u		
257-34	TP1	492-494	>38u	green yellow glass	possibly galuconite/microfossil cast

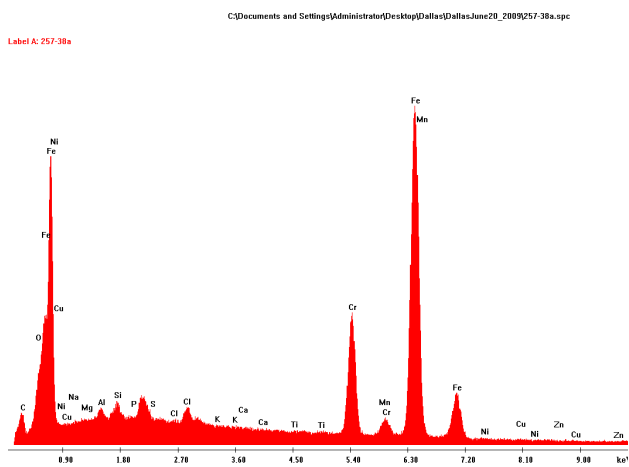
ID	TP	Range	Size	Observed	Interpretation
257-35	TP1	490-492	>38u	mungy K-spar	mungy K=spar
257-36	TP1	490-492	>38u	clear spherule	pollen C spherule, possibly with quench, D=35.8 micron, smooth surface
257-37	TP1	490-492	>38u	clear spherule	Cr, possibly part of impactor?
257-38	TP1	488-490	>38u	biotite grain	K-spar, normal cleavage, no noticeable PDFs
257-39	TP1	488-490	>38u	White grain White grain	K-spar, non-parallel lamellae <1 micron apart; some plag with same; might be a glass but no concoidal fracture
257-40	TP1	488-490	>38u		mungy SiO2, not shocked, sensitive to beam
257-41	TP1	488-490	>38u		
257-42	TP1	486-488	>38u	pollen	
257-43	TP1	486-488	>38u	clear spherule	pollen
257-44	TP1	486-488	>38u	clear spherule	pollen
257-45	TP1	484-486	>38u	glassy amber grain	organic
257-46	TP1	484-486	>38u	mungy SiO2, not shocked	
257-47	TP1	484-486	>38u	shiny black spherule	C spherule, D=40.28 micron, with possible ablation tracks and crater
257-48	TP1	484-486	>38u	clear spherule	organic
257-49	TP1	480-482	>38u	muscovite?	organic
257-50	TP1	480-482	>38u	clear spherule	pollen

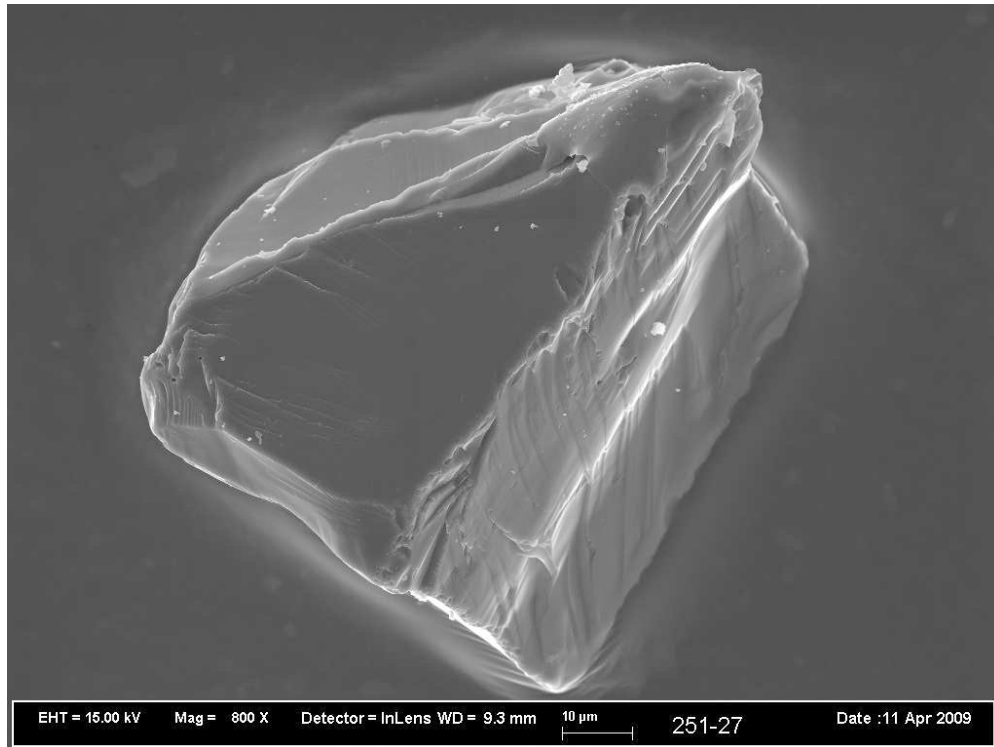
**brass analyzes as mostly Cu with little Zn

Appendix II: Minerals



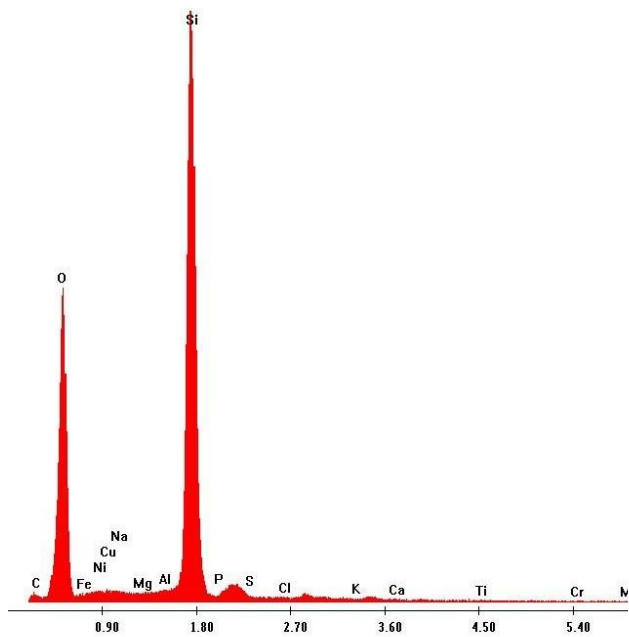
Grain 257-38 SEM micrograph and EDAX



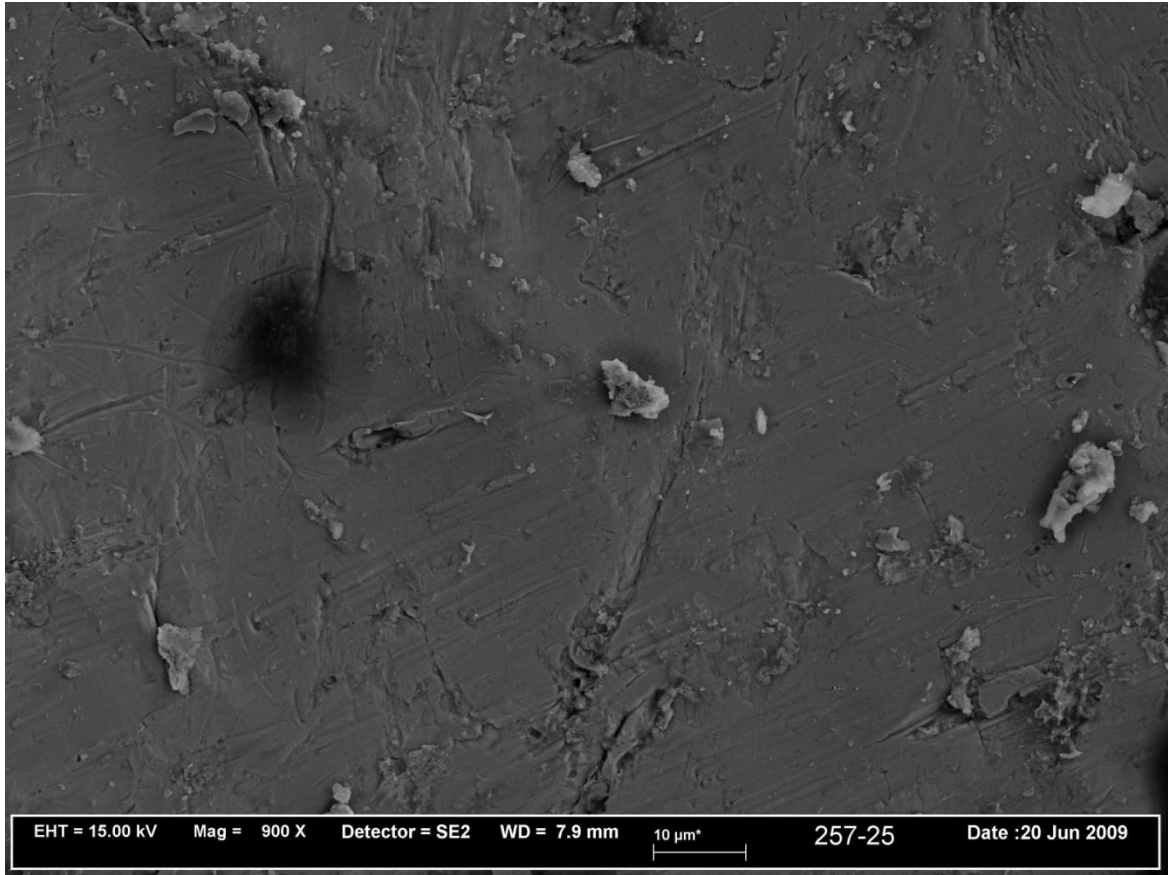


Grain 251-27

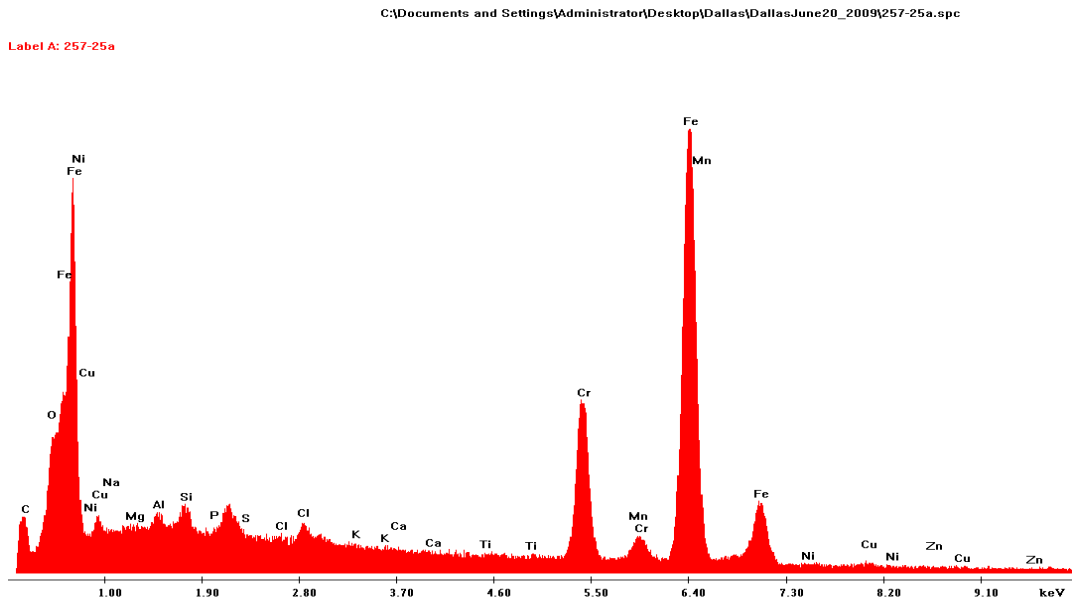
Label A: 251-27a



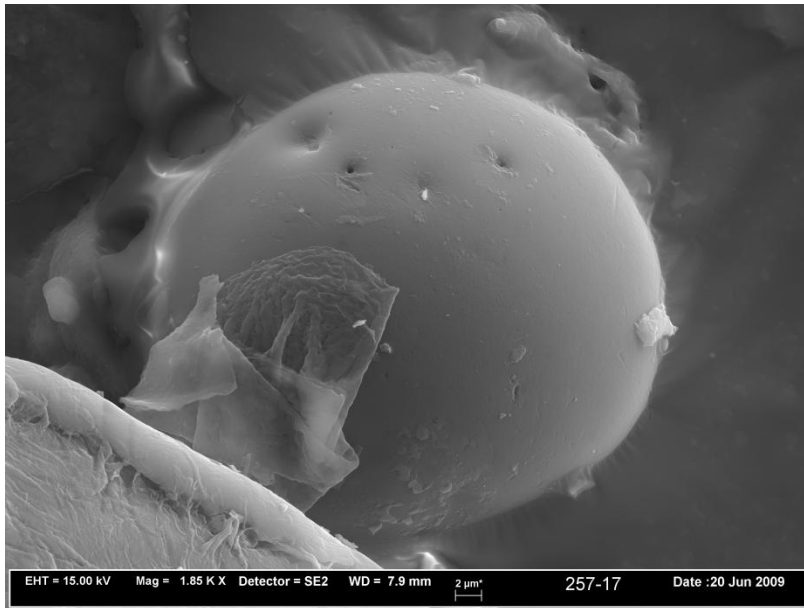
EDAX 251-27



Grain 257-25 SEM micrograph and EDAX



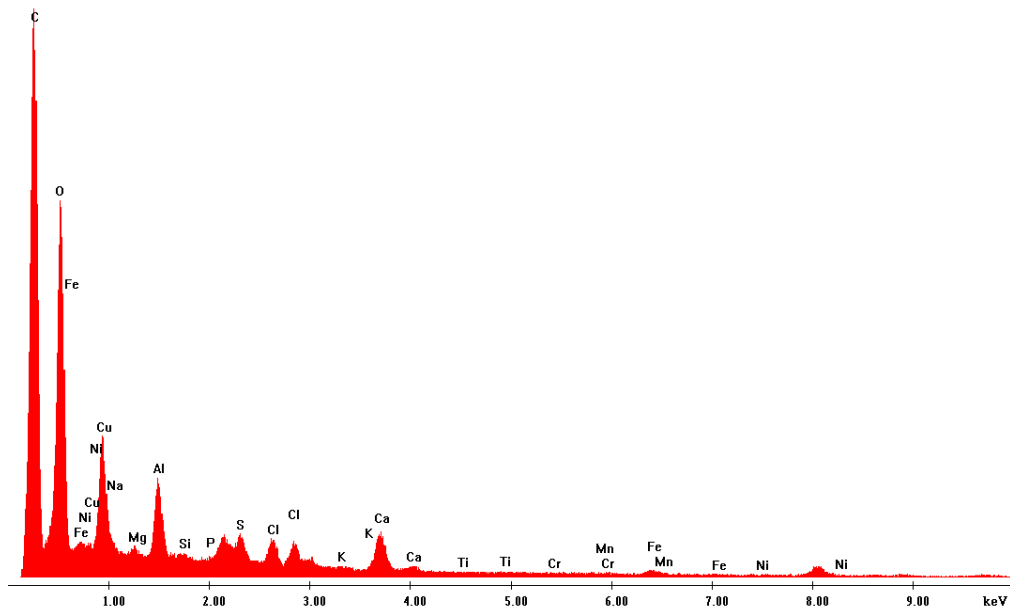
Appendix III: Spherules

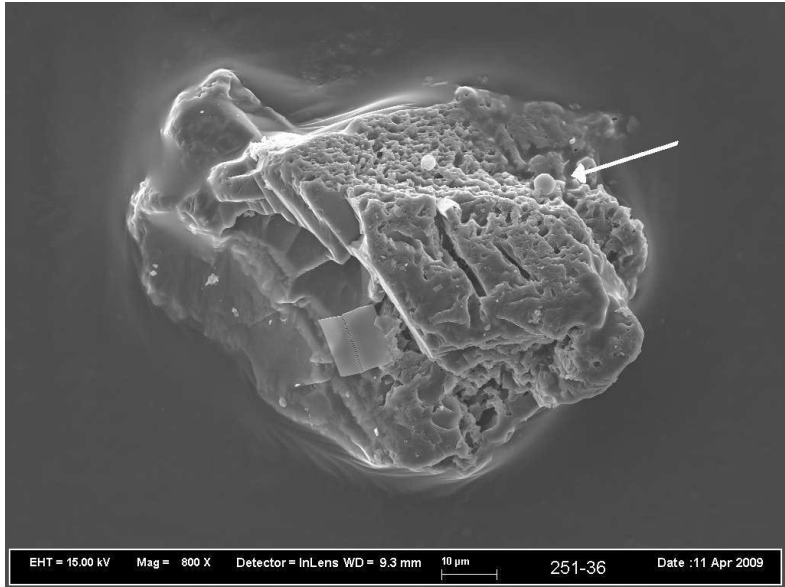


Grain 257-17 micrograph and EDAX

C:\Documents and Settings\Administrator\Desktop\Dallas\DallasJune20_2009\257-17a.spc

Label A: 257-17a





Grain 251-36 micrograph and EDAX

C:\Documents and Settings\Administrator\Desktop\Dallas\DallasMay24_2009\251-36c.spc

Label A: 251-36c

